

# One-dimensional linear analysis and numerical simulations of Alfvén waves in a force-free magnetosphere around a Kerr black hole

SHINJI KOIDE,<sup>1</sup> SOUSUKE NODA,<sup>2</sup> AND MASAOKI TAKAHASHI<sup>3</sup>

<sup>1</sup>*Department of Physics, Kumamoto University, 2-39-1, Kurokami, Kumamoto, 860-8555, JAPAN*

<sup>2</sup>*National Institute of Technology, Miyakonojo College, Miyakonojo 885-8567, Japan*

<sup>3</sup>*Department of Physics and Astronomy, Aichi University of Education, Kariya, Aichi 448-8542, Japan*

## ABSTRACT

We perform one-dimensional linear analysis and numerical simulations of the propagation of Alfvén waves in a force-free magnetosphere along magnetic field lines around a spinning black hole. We use the results to investigate the dynamic process of wave propagation and energy transport for Alfvén waves. As in a previous study using the Banados–Teitelboim–Zanelli spacetime (Koide et al. 2022), the Alfvén wave induces a fast magnetosonic wave in the case of a spinning black hole. Energy conservation is confirmed when this additional induced magnetosonic wave is considered. We also observe the reflection of the inwardly propagating Alfvén wave around the static limit, which is prohibited in theory when using the eikonal approximation.

*Keywords:* black hole physics, magnetic fields, plasmas, general relativity, Alfvén waves,  
*methods:* numerical, galaxies: active, galaxies: nuclei

## 1. INTRODUCTION

The centers of galaxies classified as active galactic nuclei (AGNs) are accompanied by drastic phenomena like the superluminal motion of knots in radio observations and flares in near-infrared, X-ray, and  $\gamma$ -ray observations (Pearson 1981; Biretta 1999; Acciari et al. 2009; Gravity Collaboration 2017). The superluminal motion of knots is explained by inhomogeneous emission from relativistic jets directed close to us and the flares are expected to be rapid energy releases from the magnetic field due to magnetic reconnection. These drastic phenomena are explained by interactions between plasma and magnetic fields around the supermassive black holes enshrined at the centers of AGNs.

The simplest approximation of the interaction between the plasma and magnetic fields is given by magnetohydrodynamics (MHD). General relativistic MHD (GRMHD) simulations have shown that the interaction between the plasma and magnetic field around black holes causes complex phenomena, including the formation of relativistic jets and flares (Koide et al. 2006; McKinney 2006; Porth et al. 2019; Ripperda et al. 2020; Nathanail et al. 2020; Hakobyan et al. 2023). These complex phenomena are made up of many elementary processes of plasma physics and the general theory of relativity. For example, GRMHD simulations have shown that the relativistic jets are powered by the Blandford–Znajek mechanism (Blandford & Znajek 1977), where the jet driving energy comes from the extracted rotational energy of the spinning black hole as a torsional Alfvén wave.

A similar phenomenon of energy extraction from spinning black holes is caused by wave scattering. That is, a wave-like scalar field, electromagnetic waves, and gravitational waves extract the rotational energy of the black hole in a process called “superradiance” (Press 1972; Teukolsky 1974). MHD waves also cause superradiance. In fact, within the force-free approximation, the magnetosonic fast wave, one of MHD waves, behaves like a scalar wave at light speed, and the fast magnetosonic wave can cause superradiance (Uchida 1997b). The other mode of MHD waves, the Alfvén wave, may also cause superradiance in the force-free limit. Uchida (1997a,b) investigated the Alfvén wave around a black hole under the force-free condition. He concluded that the superradiance of the Alfvén wave never happens within the eikonal limit because there is no reflection of the Alfvén wave near the ergosphere. Noda et al. (2020, 2022) derived a linear equation for a force-free Alfvén wave propagating along a magnetic field line around a Banados–Teitelboim–Zanelli (BTZ) black string and a Kerr black hole.

They discussed the wave scattering problem as seen by an observer who rotates with a magnetic field line (a corotating observer). By solving a stationary wave scattering problem with a finite (or long) wavelength, they concluded that the reflection rate observed by the corotating observer can exceed unity, representing superradiance, under Blandford-Znajek process conditions. To determine the reflection rate, they used the asymptotic solution of the linear equation of the Alfvén wave with Wronskian conservation.

To explore the details of superradiance energy transport in an Alfvén wave, a distinct solution around the reflection region is required. This motivates us to conduct additional linear analysis and a numerical study of an Alfvén wave around a black hole. As a first step, we study the wave propagation around a BTZ black string numerically (Koide et al. 2022). The numerical calculations reveal some interesting results regarding the dynamic processes of Alfvén waves. However, the BTZ spacetime corresponds to an infinitesimally long black string with a singularity at an infinite distance from the string, which is incompatible with real astrophysical objects.

In this paper, we investigate Alfvén wave propagation in the equatorial plane of a Kerr black hole (Fig. 1). With proper coordinates, which include a spatial coordinate along the magnetic field line, the wave equation for the Alfvén wave becomes simple and similar to the wave equation of a string. In some parameter ranges, the string corresponding to the equation is slightly strange, for example, with negative tension outside the region between the two light surfaces. This strange equation reflects surprising and interesting dynamics of the Alfvén wave around a Kerr black hole. For example, the Alfvén wave is unstable in the negative tension region, and even in the stable case, the energy of the Alfvén wave is not conserved. It is shown in this work that including the contribution of a fast magnetosonic wave induced by the Alfvén wave conserves energy as in the case of the BTZ metric (Koide et al. 2022). The induction of a fast magnetosonic wave by an Alfvén wave was also investigated by Yuan et al. (2021) for a different magnetic field configuration around a pulsar (neutron star) using special relativistic force-free electromagnetic dynamics to explain the possible energy loss mechanism in the pulsar magnetosphere. The authors suggested that the timescale of

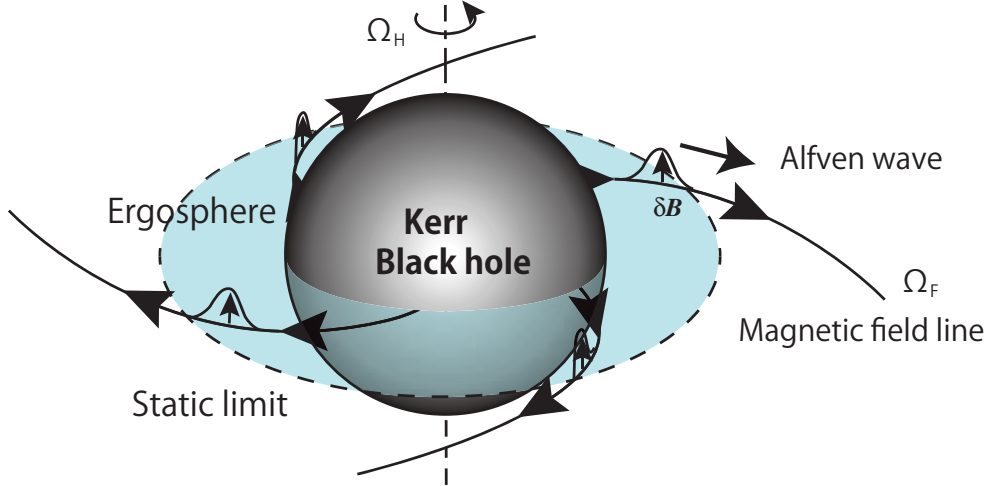


**Figure 1.** A schematic of axisymmetric Alfvén wave pulse propagations along magnetic field lines on the equatorial plane around a Kerr black hole. The dashed ring shows the static limit, which is the boundary of the ergosphere.  $\Omega_F$  and  $\Omega_H$  are constants along the stationary magnetic field line.  $\Omega_F$  corresponds to the angular velocity of the stationary magnetic field line, and  $\Omega_H$  is the angular velocity of the normal frame at the horizon.

dissipation of the Alfvén wave to a fast magnetosonic wave in the closed magnetosphere around a neutron star should be comparable to the duration of the X-ray bursts of some pulsars.

This paper is organized as follows. In Section 2, we explain the linear theory for Alfvén waves using first-order perturbation theory along stationary background magnetic field lines around a black hole. The second-order variable  $\chi$  is introduced, which describes the fast magnetosonic wave induced by the Alfvén wave. In Section 3, we investigate the conservation of energy and angular momentum for the Alfvén wave and the induced fast magnetosonic wave. In Section 4, we summarize the numerical methods, and in Section 5, we present the numerical results. We comprehensively summarize and discuss the results in Section 6. Throughout this paper, we use the natural unit system, where the speed of light and gravitational constant are unity (i.e.,  $c = 1$  and  $G = 1$ ).

## 2. BACKGROUND MAGNETOSPHERE AND ALFVÉN WAVE

We investigate the propagation of the Alfvén wave along a magnetic field line in a force-free magnetosphere around a Kerr black hole. Under the force-free condition  $J^\mu F_{\mu\nu} = 0$  ( $J^\mu$  is the 4-current density and  $F_{\mu\nu}$  is the electromagnetic field tensor), with the homogeneous Maxwell equation  $\nabla_\mu {}^*F^{\mu\nu} = 0$  ( ${}^*F^{\mu\nu}$  is the dual of  $F_{\mu\nu}$ ;  ${}^*F^{\mu\nu} = \epsilon^{\mu\nu\rho\sigma} F_{\rho\sigma}/2$ ), the electromagnetic field tensor  $F_{\mu\nu}$  is represented by the Euler potentials  $\phi_1$  and  $\phi_2$  as:

$$F_{\mu\nu} = \partial_\mu \phi_1 \partial_\nu \phi_2 - \partial_\nu \phi_1 \partial_\mu \phi_2 \quad (1)$$

as shown by Uchida (1997a,b) and used by Noda et al. (2020, 2022). The contour surfaces of the Euler potentials  $\phi_1$  and  $\phi_2$  at a certain time give the magnetic surfaces at the time as shown below. Here,  $\epsilon^{\mu\nu\rho\sigma}$  is the completely antisymmetric tensor and determined as  $\epsilon^{0123} = 1/\sqrt{-g}$  and  $g$  is the determinant of the metric tensor  $g_{\mu\nu}$ , with  $g \equiv \det(g_{\mu\nu})$ .<sup>1</sup> With Euler potentials, the homogeneous Maxwell equation  $\nabla_\mu {}^*F^{\mu\nu} = 0$  is satisfied identically. Using the inhomogeneous Maxwell equation  $\nabla_\lambda F^{\lambda\mu} = -J^\mu$  and the condition of the force-free field  $J^\mu F_{\mu\nu} = 0$  with Eq. (1), we obtain equations for  $\phi_1$  and  $\phi_2$ :

$$\partial_\lambda \phi_i \partial_\nu [\sqrt{-g} W^{\lambda\alpha\nu\beta} \partial_\alpha \phi_1 \partial_\beta \phi_2] = 0 \quad (i = 1, 2), \quad (2)$$

where  $W^{\lambda\alpha\nu\beta} = g^{\lambda\alpha} g^{\nu\beta} - g^{\lambda\beta} g^{\alpha\nu}$ .<sup>2</sup> For intuitive discussion in the following sections, we use the electric field  $\mathbf{E}$  and the magnetic field  $\mathbf{B}$ . The 4-electric field and 4-magnetic field are defined as  $E^\lambda = F^{\lambda\nu} N_\nu = -\alpha F^{\lambda 0} = -\alpha(\partial^\lambda \phi_1 \partial^0 \phi_2 - \partial^0 \phi_1 \partial^\lambda \phi_2)$  and  $B^\lambda = {}^*F^{\lambda\nu} N_\nu = -\alpha {}^*F^{\lambda 0} = \frac{1}{\sqrt{\eta}} \eta^{0\lambda\alpha\beta} \partial_\alpha \phi_1 \partial_\beta \phi_2$ , respectively, where  $\eta^{\alpha\beta\gamma\delta}$  is the Levi-Civita symbol, with  $\eta^{0123} = 1$  and  $N^\mu$  is the 4-velocity of the normal observer frame  $x^{\tilde{\mu}}$ . The spatial components of  $E^\mu$  and  $B^\mu$  give the components of the electric field  $\mathbf{E}$  and the magnetic field  $\mathbf{B}$ . The contour surface  $\phi_m$  ( $m = 1, 2$ ) at a certain time gives the magnetic surface at the time because the surface is tangent to  $\mathbf{B}$ :  $B^i \partial_i \phi_m = B^\lambda \partial_\lambda \phi_m = \frac{1}{\sqrt{\eta}} \eta^{0\lambda\alpha\beta} \partial_\alpha \phi_1 \partial_\beta \phi_2 \partial_\lambda \phi_m = 0$ .

<sup>1</sup> The sign of  $\epsilon^{\mu\nu\rho\sigma}$  is opposite to that of Noda et al. (2022)

<sup>2</sup> We note the following useful formulae concerning  $W^{\lambda\alpha\nu\beta}$ :  $W^{\lambda\alpha\mu\beta} = W^{\alpha\lambda\beta\mu} = W^{\beta\mu\alpha\lambda} = W^{\mu\beta\lambda\alpha} = -W^{\lambda\beta\mu\alpha} = -W^{\mu\alpha\lambda\beta}$ ,  $W^{\mu\nu\lambda\kappa} + W^{\mu\kappa\nu\lambda} + W^{\mu\lambda\kappa\nu} = 0$ .

2.1. *The force-free stationary background solution in Boyer–Lindquist coordinates*

The metric of the Boyer–Lindquist coordinates  $x_{\text{BL}}^\mu = (t, r, \theta, \varphi)$  is given by

$$ds^2 = g_{\mu\nu}^{\text{BL}} dx_{\text{BL}}^\mu dx_{\text{BL}}^\nu = -\alpha^2 dt^2 + \gamma_{ij} (dx_{\text{BL}}^i + \beta^i dt)(dx_{\text{BL}}^j + \beta^j dt), \quad (3)$$

where Greek indices such as  $\mu$  and  $\nu$  run from 0 to 3, while Roman indices such as  $i$  and  $j$  run from 1 to 3,  $\alpha^2 = -g_{tt} + \gamma_{ij}\beta^i\beta^j = \frac{\Sigma\Delta}{A}$ ,  $\gamma_{rr} = \frac{\Sigma}{\Delta}$ ,  $\gamma_{\theta\theta} = \Sigma$ ,  $\gamma_{\phi\phi} = \frac{A}{\Sigma}\sin^2\theta \equiv R^2$ ,  $\gamma_{ij} = 0, (i \neq j)$ ,  $\beta^\phi = -\Omega$ ,  $\beta^r = \beta^\theta = 0$ ,  $\Delta = r^2 - 2Mr + a^2$ ,  $\Sigma = r^2 + a^2\cos^2\theta$ ,  $A = (r^2 + a^2)^2 - a^2\Delta\sin^2\theta$ , and  $\Omega = -\frac{g_{r\varphi}^{\text{BL}}}{g_{\varphi\varphi}^{\text{BL}}} = \frac{2Mar}{A}$ . Here, the spin parameter of a black hole  $a$  is given by  $a = J/M$ , where  $M$  and  $J$  are the mass and angular momentum of the black hole, respectively. The dimensionless spin parameter  $a_*$  is given by  $a_* = a/M$ . The determinant of the metric tensor for the Boyer–Lindquist coordinates ( $g_{\mu\nu}^{\text{BL}}$ ) is given by  $g_{\text{BL}} \equiv \det(g_{\mu\nu}^{\text{BL}}) = -\Sigma^2\sin^2\theta$ , and the 4-velocity of the normal observer (Zero-Angular-Momentum Observer: ZAMO) is given by

$$N^\lambda = \left( \frac{1}{\alpha}, -\frac{\beta^i}{\alpha} \right), N_\lambda = (-\alpha, 0, 0, 0). \quad (4)$$

Using Eq. (2), we obtain the steady-state solution of the force-free magnetic field around the equatorial plane ( $\theta \sim \pi/2$ ) of the black hole

$$\bar{\phi}_1 = -\cos\theta, \quad \bar{\phi}_2 = \int \frac{I r^2}{\Delta} dr + \varphi - \Omega_{\text{F}} t, \quad (5)$$

where  $\bar{\phi}_i$  ( $i = 1, 2$ ) represents the steady-state solution, and  $\Omega_{\text{F}}$  and  $I$  are constants along a field line. These constants mean that  $\Omega_{\text{F}}$  is the angular velocity of the magnetic field line, and  $I$  is the total current, which is obtained from the regularity of  $F^{\mu\nu}F_{\mu\nu}$  at the black hole horizon as,

$$I = \frac{2M}{r_{\text{H}}}(\Omega_{\text{H}} - \Omega_{\text{F}}). \quad (6)$$

The solution given by Eq. (5) corresponds to the field of the magnetic monopole around the equatorial plane. Here, the strength of the stationary magnetic field is normalized without loss of generality. Note that  $\phi_m$  ( $m = 1, 2$ ) corresponds to the stream function and the contour surface of  $\bar{\phi}_m$  at a certain time represents the steady-state magnetic surfaces. In the present case,  $\bar{\phi}_1 = -\cos\theta = 0$

represents the steady magnetic surface along the equatorial plane. The magnetic flux surface  $\bar{\phi}_2 = \text{const.}$  is vertical to the equatorial plane and contains the magnetic field line on the equatorial plane. The corotating Killing vector of the field line,  $\xi_{(F)}^\nu \equiv \xi_{(t)}^\nu + \Omega_F \xi_{(\varphi)}^\nu$  is parallel to the 4-velocity of an observer corotating with the magnetic field line, where  $\xi_{(t)}^\nu$  is the Killing vector in the time direction and  $\xi_{(\phi)}^\nu$  is the Killing vector in the azimuthal direction. The norm of  $\xi_{(F)}^\nu$  is

$$\Gamma \equiv g_{\mu\nu}^{\text{BL}} \xi_{(F)}^\mu \xi_{(F)}^\nu = -\alpha^2 + R^2(\Omega - \Omega_F)^2, \quad (7)$$

where the roots of  $\Gamma = 0$  give the location of the inner and outer light surfaces.

## 2.2. Magnetic natural frame

To simplify the form of the calculations, we utilize the coordinates  $(T, X, \rho, z)$ , defined as

$$T = t, \quad (8)$$

$$X = r, \quad (9)$$

$$\rho = \varphi - \int \frac{IX^2}{\Delta} dr, \quad (10)$$

$$\Psi = -\cos \theta. \quad (11)$$

The coordinate frame does not rotate, although it is similar to the coordinate frame used by [Noda et al. \(2022\)](#), which rotates with the same angular velocity as the magnetic field lines. In this coordinate system,  $X$  is the coordinate along the magnetic field line, so we call this coordinate system  $(T, X, \Psi, \rho)$  the “magnetic natural frame”. The contravariant component of the metric tensor of the magnetic natural frame  $(T, X, \Psi, \rho)$  is as follows:

$$(g^{\mu\nu}) = \begin{pmatrix} g_{\text{BL}}^{tt} & 0 & 0 & g_{\text{BL}}^{\varphi t} \\ 0 & g_{\text{BL}}^{rr} & 0 & \frac{IX^2}{\Delta} g_{\text{BL}}^{rr} \\ 0 & 0 & g_{\text{BL}}^{\theta\theta} \sin^2 \theta & 0 \\ g_{\text{BL}}^{\varphi t} & \frac{IX^2}{\Delta} g_{\text{BL}}^{rr} & 0 & g_{\text{BL}}^{\varphi\varphi} + \left(\frac{IX^2}{\Delta}\right)^2 g_{\text{BL}}^{rr} \end{pmatrix} = \begin{pmatrix} -\frac{1}{\alpha^2} & 0 & 0 & -\frac{\Omega}{\alpha^2} \\ 0 & \frac{\Delta}{\Sigma} & 0 & \frac{IX^2}{\Sigma} \\ 0 & 0 & \frac{\sin^2 \theta}{\Sigma} & 0 \\ -\frac{\Omega}{\alpha^2} & \frac{IX^2}{\Sigma} & 0 & \frac{1}{R^2} - \frac{\Omega}{\alpha^2} + \frac{I^2 X^4}{\Delta \Sigma} \end{pmatrix}. \quad (12)$$

The determinant of the matrix  $(g_{\mu\nu})$  is given by  $g = \det(g_{\mu\nu}) = -\Sigma^2$ . In the magnetic natural frame, the steady-state force-free solution given by Eq. (5) is simply

$$\bar{\phi}_1 = \Psi, \quad \bar{\phi}_2 = \rho - \Omega_F T. \quad (13)$$

### 2.3. Wave equation for the Alfvén wave

In the background magnetosphere given by Eq. (13), we consider a perturbation of the magnetic field; that is, the propagation of Alfvén waves. We already know that an Alfvén wave induces a fast wave represented by a second-order perturbation, as suggested by the calculations in BTZ spacetime (Koide et al. 2022). Therefore, we should consider not only the Alfvén wave but also the fast wave using second-order perturbation. The infinitesimally small perturbation to the Euler potential  $\phi_i \longrightarrow \bar{\phi}_i + \delta\phi_i$  is given by the displacement (polarization) vector  $\zeta^\lambda$  as  $\delta\phi_i = \zeta^\lambda \partial_\lambda \phi_i$ . First, we consider the Alfvén wave with a first-order perturbation. We focus on a pure Alfvén wave propagating on the magnetic surface at the equatorial plane ( $\Psi = -\cos\theta = 0$ ) and oscillating perpendicularly to the magnetic surface:  $\delta\zeta^\lambda = (0, 0, \delta\zeta^\Psi, 0)$ . This wave is the “pure” Alfvén wave because the polarization direction of the oscillation  $\delta\zeta^\lambda$  is perpendicular to that of the propagation which is parallel to the equatorial plane  $\Psi = \bar{\phi}_1 = 0$ . Then, the perturbed Euler potentials are

$$\phi_1 = \bar{\phi}_1 + \delta\phi_1 = \Psi + \delta\phi_1, \quad \phi_2 = \bar{\phi}_2 = \rho - \Omega_F T, \quad (14)$$

because  $\delta\phi_2 = \delta\zeta^\mu \partial_\mu \bar{\phi}_2 = \delta\zeta^\Psi \partial_\Psi (\rho - \Omega_F T) = 0$ . Hereafter, we denote the stationary background (zeroth-order) term, first-order perturbation, second-order perturbation,  $\dots$  of a variable  $A$  as  $\bar{A}$ ,  $\delta A$ ,  $\delta^2 A$ ,  $\dots$ , i.e.,  $A = \bar{A} + \delta A + \delta^2 A + \dots$ . Without loss of generality, we assume the perturbation for the Alfvén wave is axisymmetric, i.e., the perturbation is independent of  $\rho$ :

$$\delta\phi_1 = \psi(T, X, \Psi), \quad (15)$$

where the Alfvén wave propagates along a magnetic field line and never interacts with Alfvén waves propagating along other magnetic field lines.

In nonrotating natural coordinates, the linearization of Eq. (2) with  $i = 2$  yields

$$\partial_\lambda (\sqrt{-g} W^{\lambda\alpha\mu\beta} \partial_\alpha \psi \partial_\beta \bar{\phi}_2) \partial_\mu \bar{\phi}_1 + \partial_\lambda (\sqrt{-g} W^{\lambda\alpha\mu\beta} \partial_\alpha \bar{\phi}_1 \partial_\beta \bar{\phi}_2) \partial_\mu \psi = 0, \quad (16)$$



and can be calculated easily as

$$\partial_\lambda(\sqrt{-g}Z^{\lambda\alpha}\partial_\alpha\psi) = 0, \quad (17)$$

where  $Z^{\lambda\alpha} = W^{\lambda\alpha\mu\beta}\partial_\mu\bar{\phi}_2\partial_\beta\bar{\phi}_2 = W^{\lambda\alpha\rho\rho} - \Omega_F(W^{\lambda\alpha\rho T} + W^{\lambda\alpha T\rho}) + \Omega_F^2W^{\lambda\alpha TT}$ .<sup>3</sup> Using the variables  $\lambda = -\sqrt{-g}Z^{TT}$ ,  $S = \sqrt{-g}Z^{XX}$ ,  $K = \sqrt{-g}Z^{\Psi\Psi}$ , and  $V = -\sqrt{-g}Z^{TX}$ , we rewrite Eq. (17) as

$$\lambda\frac{\partial^2\psi}{\partial T^2} - \frac{\partial}{\partial X}\left(S\frac{\partial\psi}{\partial X}\right) + \frac{\partial}{\partial T}\left(V\frac{\partial\psi}{\partial X}\right) + \frac{\partial}{\partial X}\left(V\frac{\partial\psi}{\partial T}\right) + K\psi = 0. \quad (18)$$

This equation is identified by the equation of displacement of a string with a nonuniform line density  $\lambda$  and nonuniform tension  $S + \frac{V^2}{\lambda}$ , which moves with a nonuniform velocity  $\frac{V}{\lambda}$  and is bounded by springs with a spring constant per unit length  $K$ .<sup>4</sup> Using the metric tensor of the nonrotating natural coordinates (Eq. (12)) and the nature of the perturbation ( $\partial_\Psi^2\psi = -\psi$ ), we obtain the explicit expressions for the parameters of the analogous string,

$$\lambda = \frac{1}{\alpha^2}\left(\frac{\Sigma}{R^2} + \frac{I^2X^4}{\Delta}\right), \quad (19)$$

$$S = \frac{1}{\sin^2\theta}[\alpha^2 - R^2(\Omega_F - \Omega)^2] = \frac{-\Gamma}{\sin^2\theta}, \quad (20)$$

$$K = \frac{1}{\Delta}\left[\alpha^2 - R^2(\Omega_F - \Omega)^2 + \frac{I^2X^4\sin^2\theta}{\Sigma}\right] = \frac{\sin^2\theta}{\Delta}\left(S + \frac{I^2X^2}{\Sigma}\right), \quad (21)$$

$$V = \frac{IX^2}{\alpha^2}(\Omega_F - \Omega), \quad (22)$$

where we have the identity  $V^2 + \lambda S = \frac{\Sigma K}{\sin^2\theta}$ . Equation (20) shows that the string analogous to Eq. (18) is strange because the tension  $S + \frac{V^2}{\lambda} = \frac{\Sigma}{\lambda}K$  becomes negative outside the region between the inner and outer light surfaces, as  $S = -\Gamma$  at the equatorial plane.

#### 2.4. Dispersion relation of the Alfvén wave and instability

In the eikonal limit, that is, the short wavelength limit, Eq. (18) yields the dispersion relation of the Alfvén wave, Eq. (A1). Equation (A1) reveals not only the propagation of the Alfvén wave but

<sup>3</sup>  $Z^{\mu\nu}$  is proportional to the projection operator onto the constant- $\bar{\phi}_2$  hypersurface,  $\mathcal{P}^{\mu\nu} \equiv g^{\mu\nu} - \partial^\mu\bar{\phi}_2\partial^\nu\bar{\phi}_2/|\partial\bar{\phi}_2|^2 = |\partial\bar{\phi}_2|^{-2}Z^{\mu\nu}$ , where  $|\partial\bar{\phi}_2| = \sqrt{\partial_\mu\bar{\phi}_2\partial^\mu\bar{\phi}_2}$ .

<sup>4</sup> Because Eq. (18) is expressed by  $\lambda\left(\frac{\partial}{\partial T} + \frac{V}{\lambda}\frac{\partial}{\partial X}\right)^2\psi - \frac{\partial}{\partial X}\left[\left(S + \frac{V^2}{\lambda}\right)\frac{\partial\psi}{\partial X}\right] + K\psi + \frac{\partial V}{\partial X}\left(\frac{\partial\psi}{\partial T} + \frac{V}{\lambda}\frac{\partial\psi}{\partial X}\right) = 0$ .

When we neglect the nonuniformity of  $V$ , we obtain the equation of a moving string,  $\lambda\left(\frac{\partial}{\partial T} + \frac{V}{\lambda}\frac{\partial}{\partial X}\right)^2\psi - \frac{\partial}{\partial X}\left[\left(S + \frac{V^2}{\lambda}\right)\frac{\partial\psi}{\partial X}\right] + K\psi = 0$ .

also the instability of the wave outside the outer light surface. In Appendix A, it is shown that the Alfvén wave is stable over the entire radial range ( $r_{\text{H}} < X < \infty$ ) when  $\Omega_{\text{F}} < \frac{2M}{2M + r_{\text{H}}}|\Omega_{\text{H}}| \equiv \Omega_{\text{c}}$ . Otherwise ( $\Omega_{\text{F}} > \Omega_{\text{c}}$ ), the Alfvén wave is unstable at  $X > r_{\text{m}}$ , where  $X = r_{\text{m}}$  is the solution for  $K = 0$ . In the numerical calculations in this paper, we use the parameters of the case where the Alfvén wave is stable over the entire radial range ( $\Omega_{\text{F}} < \Omega_{\text{c}}$ ).

### 2.5. *Perturbations of the Alfvén wave and induced wave*

The induction of a fast wave by an Alfvén wave is explained by a relativistic mechanism, where the angular momentum of the Alfvén wave changes in time (Fig. 2). The Poynting flux of the Alfvén wave is directed in the propagation direction of the wave. The Poynting flux is proportional to the electromagnetic momentum density of the Alfvén wave. Then, generally speaking, the Alfvén wave propagating along the magnetic field line has its angular momentum as a second-order perturbation. Therefore, if the magnetic field line is curved azimuthally ( $I \neq 0$ ) or rotates ( $\Omega_{\text{F}} \neq 0$ ), a torque on the Alfvén wave is required so that the Alfvén wave traces the magnetic field line. This means the force-free condition is broken at second order and the azimuthal component of the Lorentz force becomes finite. To change the angular momentum of the Alfvén wave, the Alfvén wave should be subject to an external torque to trace the rotating magnetic field line. Thus, we take into account additional first- and second-order perturbations  $\delta^2\phi_1$ ,  $\delta^2\phi_2$  as

$$\phi_1 = \bar{\phi}_1 + \delta\phi_1 = \Psi + \psi(T, X, \Psi), \quad (23)$$

$$\phi_2 = \bar{\phi}_2 + \delta^2\phi_2 = \rho - \Omega_{\text{F}}T + \chi(T, X, \Psi), \quad (24)$$

where  $\chi \equiv \delta^2\phi_2 = \delta^2\zeta^\lambda\partial_\lambda\bar{\phi}_2 = \delta^2\zeta^\lambda\partial_\lambda(\rho - \Omega_{\text{F}}T) = \delta^2\zeta^\rho - \Omega_{\text{F}}\delta^2\zeta^T$ . This perturbation corresponds to the fast wave because the polarization of the oscillation of the magnetic surface  $\delta^2\zeta^i = (0, 0, \delta^2\zeta^\rho)$  is parallel to the propagation surface of the wave, i.e. the equatorial plane. Using  $\chi$ , we find that the force-free condition is recovered with the second-order perturbation. For simplicity, we assume  $\partial_\Psi\chi = \partial_\Psi^2\chi = 0$  without any contradiction.

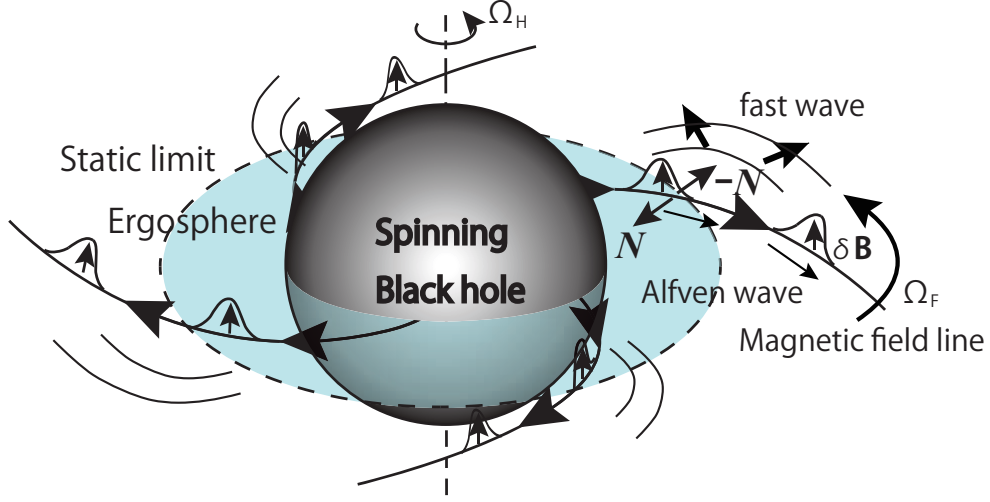


**Figure 2.** A schematic of the Alfvén wave and the wave induced by the Alfvén wave propagation along curved rotating field lines around a spinning black hole.  $N$  shows the force exerted by the background magnetic field line on the Alfvén wave. The reaction of the force produces an induced wave oscillating in the azimuthal direction of the magnetic field line.

From Eq. (2), the time evolution equation of  $\chi$  is obtained as

$$\frac{1}{\sqrt{-g}}\partial_\lambda(\sqrt{-g}g^{\Psi\Psi}g^{\lambda\beta}\partial_\beta\chi) = s, \quad (25)$$

where

$$s \equiv \frac{1}{\sqrt{-g}}\partial_\lambda(\sqrt{-g}Y^{\lambda\alpha\mu}\partial_\alpha\psi\partial_\mu\psi) = \frac{1}{\sqrt{-g}}[\partial_T\Theta\partial_X\psi - \partial_X\Theta\partial_T\psi] \quad (26)$$

with  $Y^{\lambda\alpha\mu} \equiv W^{\lambda\alpha\mu\nu}\partial_\nu\bar{\phi}_2 = W^{\lambda\alpha\mu\rho} - \Omega_F W^{\lambda\alpha\mu T}$  and  $\Theta \equiv \sqrt{-g}Y^{T\alpha X}\partial_\alpha\psi = -\frac{IX^2}{\alpha^2}\partial_T\psi - R^2(\Omega_F - \Omega)\partial_X\psi$  (see the derivation in Appendix C). The right-hand side of Eq. (25),  $s$ , is recognized as the source term of the wave equation of  $\chi$  as the second-order perturbation  $\sim \psi^2$ . Therefore,  $\chi$  in Eq. (25) represents the wave induced by the Alfvén wave. Introducing  $\chi$ , we confirm that the force-free condition holds. The linear inhomogeneous equation (Eq. (25)) shows the wave described by  $\chi$  propagates isotropically in space as by a fast wave (Bellman 2006), while the complex formalism of the homogeneous linear equation of  $\psi$  (Eq. (16)) suggests strong anisotropy of the wave described by  $\psi$ , which is a characteristic property of an Alfvén wave.

### 3. ENERGY AND ANGULAR MOMENTUM CONSERVATION

In this section, we consider the energy and angular momentum transport of the Alfvén wave and the fast mode (the second-order perturbation).

The Maxwell equations yield the energy-momentum conservation law,

$$\nabla_\nu T^{\mu\nu} = -f_L^\mu, \quad (27)$$

where  $T^{\mu\nu} = F^\mu{}_\sigma F^{\nu\sigma} - \frac{1}{4}g^{\mu\nu}F_{\lambda\kappa}F^{\lambda\kappa}$  is the energy-momentum tensor of the electromagnetic field and  $f_L^\mu = J^\nu F^\mu{}_\nu$  is the 4-Lorentz force density. Here,  $f_L^\mu = 0$  is the “force-free condition”. For the background equilibrium, we can confirm the Lorentz force of the equilibrium vanishes because the 4-current density of the equilibrium vanishes,  $\bar{f}_\mu^L = 0$ . We can also confirm that the Lorentz force with respect to the first-order perturbation of Alfvén wave vanishes,  $\delta f_\mu^L = 0$ . It is noted that  $\delta J^\rho = \delta J^\Psi = 0$ . As concluded in the previous study in BTZ space-time (Koide et al. 2022), we have to take into account the second-order contribution to the energy and angular momentum, because the first order always vanishes as shown later. Furthermore, as we consider only the first-order perturbation of the Alfvén wave, the second order of the right-hand side of Eq. (27) never vanishes:  $\delta^{1+1}f_L^\mu \neq 0$ . When we consider the second-order perturbation that corresponds to the fast mode, the right-hand side of Eq (27) vanishes:  $\delta^2 f_L^\mu = \delta^{1+1}f_L^\mu + \delta^{0+2}f_L^\mu = 0$ .

To investigate the energy and momentum transfer due to the Alfvén wave, we consider the perturbation of  $T^{\mu\nu}$  at first or higher order. When we assume Eqs. (23) and (24), the first order of  $T^{\mu\nu}$  is calculated as

$$\delta T_\nu^\mu = \delta F^{\mu\lambda} \bar{F}_{\nu\lambda} + \bar{F}^{\mu\lambda} \delta F_{\nu\lambda} - \frac{1}{2}g_\nu^\mu \bar{F}^{\lambda\kappa} \delta F_{\lambda\kappa}, \quad (28)$$

for which a detailed derivation is provided in Appendix B. The second- and third-order terms on the right-hand side of Eq. (28) vanish because of  $\partial_\Psi \psi = 0$ . The first term on the right-hand side of Eq. (28) is

$$\delta F^{\mu\lambda} \bar{F}_{\Psi\lambda} = \delta F^{\mu\rho} \bar{F}_{\Psi\rho} = -\delta F^{\mu\rho} = -W^{\mu\lambda\rho\rho}, \quad (29)$$

which is non-vanishing when either  $\mu = \Psi$  or  $\nu = \Psi$  holds. Thus, when neither  $\mu = \Psi$  or  $\nu = \Psi$ , we have

$$\delta T_\nu^\mu = 0. \quad (30)$$

Equation (30) shows that the second-order perturbation should be considered when investigating the energy transport of the linear Alfvén wave. If the force-free condition of the second-order perturbation is broken, the energy and angular momentum of the Alfvén wave are not conserved. To verify the conservation of energy and angular momentum, we evaluate the force-free condition up to second order in the energy density and angular momentum density of the Alfvén wave.

For the second-order perturbation, we have

$$\delta^2 J^\mu = \frac{1}{\sqrt{-g}} \partial_\nu (\sqrt{-g} \delta^2 F^{\mu\nu}) = \frac{1}{\sqrt{-g}} \partial_\nu (\sqrt{-g} W^{\mu\Psi\nu\kappa} \partial_\kappa \chi). \quad (31)$$

The non-zero component of  $\delta^2 J^\mu$  is

$$\delta^2 J^\Psi = \frac{1}{\sqrt{-g}} \partial_\nu (\sqrt{-g} g^{\Psi\Psi} g^{\nu\kappa} \partial_\kappa \chi). \quad (32)$$

Using Eq. (25), we find that the inhomogeneous term of the second-order perturbation of the energy conservation law (27) is written as

$$\begin{aligned} \delta^2 f_T &= \delta^2 J^\nu \bar{F}_{T\nu} + \delta J^\nu \delta F_{T\nu} = \delta^2 J^\Psi \bar{F}_{T\Psi} + \delta J^\nu \delta F_{T\nu} \\ &= \frac{1}{\sqrt{-g}} \Omega_F [\partial_\nu (\sqrt{-g} g^{\Psi\Psi} g^{\nu\kappa} \partial_\kappa \chi) + \partial_\nu (\sqrt{-g} Y^{\mu\lambda\nu} \partial_\lambda \psi \partial_\mu \psi)] = 0, \end{aligned} \quad (33)$$

which represents the fast wave induced by the Alfvén wave (the first-order perturbation). Thus, we have shown the total energy of the Alfvén wave and fast wave is conserved when considering second-order perturbations.

### 3.1. The energy and angular momentum conservation laws in natural coordinates

When  $\xi^\mu$  is the Killing vector, we have the conservation law

$$\frac{\partial}{\partial x^0} (\xi_\nu T^{0\nu}) + \frac{1}{\sqrt{-g}} \frac{\partial}{\partial x^i} (\sqrt{-g} \xi_\nu T^{i\nu}) = \frac{1}{\sqrt{-g}} \partial_\mu (\sqrt{-g} T^{\mu\nu}) = \nabla_\mu (\xi_\nu T^{\mu\nu}) = -\xi^\nu f_\nu^L. \quad (34)$$

When  $\xi^\nu f_\nu^L$  vanishes,  $\xi_\nu T^{0\nu}$  represents the density of the conserved value and  $\xi_\nu T^{i\nu}$  represents the density of the conserved quantity flux.

For the time-like Killing vector  $\xi_{(T)}^\mu = (1, 0, 0, 0)$  and the axial Killing vector  $\xi_{(\rho)}^\mu = (0, 0, 0, 1)$  in magnetic natural coordinates, we have the energy and angular momentum conservation laws

$$\frac{\partial S^T}{\partial T} + \frac{1}{\sqrt{-g}} \frac{\partial}{\partial X} (\sqrt{-g} S^X) + \frac{1}{\sqrt{-g}} \frac{\partial}{\partial \Psi} (\sqrt{-g} S^\Psi) = f_T^L = 0, \quad (35)$$

$$\frac{\partial M^T}{\partial T} + \frac{1}{\sqrt{-g}} \frac{\partial}{\partial X} (\sqrt{-g} M^X) + \frac{1}{\sqrt{-g}} \frac{\partial}{\partial \Psi} (\sqrt{-g} M^\Psi) = -f_\rho^L = 0, \quad (36)$$

where we assume axisymmetry and  $z$ -direction translation symmetry, and  $S^\mu = -\xi_{(T)}^\nu T^{\mu\nu}$  and  $M^\mu = \xi_{(\rho)}^\nu T^{\mu\nu}$  are the 4-energy flux and 4-angular momentum flux, respectively, up to second order.

We now consider the energy density and energy flux to determine the energy conservation law on the equatorial plane around a black hole. The Killing vector for the energy conservation law is  $\xi_{(T)}^\mu = (1, 0, 0, 0)$ . Thus, the 4-energy flux density is

$$S^\mu = -\xi_{(T)}^\nu T_\nu^\mu = -T_T^\mu. \quad (37)$$

The energy conservation law is expressed as

$$\nabla_\mu S^\mu = \frac{1}{\sqrt{-g}} \partial_\mu (\sqrt{-g} S^\mu) = \xi_{(T)}^\nu f_\nu^L = f_T^L = 0. \quad (38)$$

Hence, we have the energy density of the equilibrium, first-, and second-order perturbations with respect to the linear Alfvén wave (with  $\delta^{1+1}$ ) and the second-order fast wave (with  $\delta^{2+0}$ ),

$$\bar{S}^T = g^{\Psi\Psi} (g^{\rho\rho} - \Omega_F^2 g^{TT}), \quad (39)$$

$$\delta S^T = 0, \quad (40)$$

$$\delta^2 S^T = \delta^{1+1} S^T + \delta^{2+0} S^T, \quad (41)$$

where

$$\delta^{1+1} S^T = \frac{1}{\sqrt{-g}} \left[ \frac{\lambda}{2} (\partial_T \psi)^2 + \frac{S}{2} (\partial_X \psi)^2 + \frac{2}{\alpha^2} \Omega_F \partial_T \psi \partial_X \psi \right], \quad (42)$$

$$\delta^{2+0} S^T = \frac{I}{\sqrt{-g}} \partial_X \chi - \frac{1}{\alpha^2} \Omega_F \partial_T \chi. \quad (43)$$

In the numerical calculations, we use the above formulation (Eqs. (41)-(43)) with the tortoise coordinates (see Appendix E). We can obtain the energy flux density of the equilibrium, first-, and

second-order perturbations of the linear Alfvén wave,

$$\bar{S}^X = I\Omega_F, \quad (44)$$

$$\delta S^X = 0, \quad (45)$$

$$\delta^2 S^X = -\partial_T \psi Y^{X\lambda\rho} \partial_\lambda \psi - W^{\Psi\Psi X\rho} \partial_T \chi + \Omega_F W^{\Psi\Psi X X} \partial_X \chi = \delta^{1+1} S^X + \delta^{2+0} S^X, \quad (46)$$

$$\delta^2 S^\Psi = -\partial_\Psi \psi (Y^{\Psi\Psi\rho} \partial_T \psi + \Omega_F Y^{\Psi\Psi X} \partial_X \psi) = 0, \quad (47)$$

where

$$\delta^{1+1} S^X = -\frac{1}{\Sigma} \partial_T \psi \left[ (\alpha^2 + R^2 \Omega (\Omega_F - \Omega)) \partial_X \psi - \frac{\Sigma \Omega I}{\alpha^2} \partial_T \psi \right], \quad (48)$$

$$\delta^{2+0} S^X = -\frac{I}{\Sigma} \partial_T \chi + \Omega_F \frac{\Delta}{\Sigma X^2} \partial_X \chi. \quad (49)$$

Eventually, we obtain the energy conservation law of the Alfvén wave and the induced fast mode,

$$\frac{\partial}{\partial T} \delta^2 e^\infty + \frac{1}{\sqrt{-g}} \frac{\partial}{\partial X} (\sqrt{-g} \delta^2 S_P) = 0, \quad (50)$$

where  $\delta^2 e^\infty = \delta^{1+1} e^\infty + \delta^{2+0} e^\infty$ ,  $\delta^2 S_P = \delta^{1+1} S_P + \delta^{2+0} S_P$ ,  $\delta^{1+1} e^\infty = \delta^{1+1} S^T$ ,  $\delta^{2+0} e^\infty = \delta^{2+0} S^T$ ,  $\delta^{1+1} S_P = \delta^{1+1} S^X$ , and  $\delta^{2+0} S_P = \delta^{2+0} S^X$ . In the numerical calculations, we use the formulation (Eqs. (46)–(49)) with the tortoise coordinates (see Appendix E).

Next, we discuss the conservation law of the angular momentum. The axial Killing vector  $\xi_{(\rho)}^\mu = (0, 0, 0, 1)$  yields the 4-angular momentum flux density  $M^\mu = \xi_{(\rho)}^\nu T_\nu^\mu = F^{\mu\lambda} F_{\rho\lambda}$  ( $\mu \neq \rho$ ), and we obtain the angular momentum conservation law in the nonrotating natural coordinates,

$$\nabla_\mu M^\mu = \frac{1}{\sqrt{-g}} \partial_\mu (\sqrt{-g} M^\mu) = \xi_{(\rho)}^\mu f_\mu^L = f_\rho^L. \quad (51)$$

We evaluate the angular momentum and the Lorentz force density up to the second order:

$$\delta^2 M^\mu = \delta F^{\mu\lambda} \delta F_{\rho\lambda} + \delta^2 F^{\mu\lambda} \bar{F}_{\rho\lambda} + \bar{F}^{\mu\lambda} \delta^2 F_{\rho\lambda} = -Y^{\mu\kappa\lambda} \partial_\kappa \psi \partial_\lambda \psi + W^{\Psi\Psi\mu\kappa} \partial_\kappa \chi, \quad (52)$$

$$\begin{aligned} \delta^2 f_\rho^L &= \delta J^\mu \delta F_{\rho\mu} + \delta^2 J^\nu \bar{F}_{\rho\mu} + \bar{J}^\nu \delta^2 F_{\rho\mu} = -\frac{1}{\sqrt{-g}} \partial_\nu (\sqrt{-g} Y^{\mu\lambda\nu} \partial_\kappa \psi \partial_\lambda \psi) - \delta^2 J^\Psi \\ &= \frac{1}{\sqrt{-g}} \partial_\nu (\sqrt{-g} Y^{\nu\lambda\mu} \partial_\lambda \psi \partial_\nu \psi) - \frac{1}{\sqrt{-g}} \partial_\nu (\sqrt{-g} W^{\Psi\Psi\nu\kappa} \partial_\kappa \chi). \end{aligned} \quad (53)$$

Equation (51) yields

$$\delta^2 f_\rho^L = \frac{1}{\sqrt{-g}} \partial_\nu (\sqrt{-g} Y^{\nu\lambda\mu} \partial_\lambda \psi \partial_\nu \psi) - \frac{1}{\sqrt{-g}} \partial_\nu (\sqrt{-g} W^{\Psi\nu\kappa} \partial_\kappa \chi) = 0, \quad (54)$$

which is identical to the equation for  $\chi$  (Eq. (25)). When and only when  $I$ ,  $\Omega_F$ , and  $a_*$  are all zero, the first term of the central part of Eq. (54) vanishes (see the detailed calculation in Eq. (B25)). In the case of  $I = 0$ ,  $\Omega_F = 0$ , or  $a_* = 0$ , the Alfvén wave never induces the fast wave.

Eventually, we obtain the angular momentum conservation law with respect to the Alfvén wave and the induced fast mode,

$$\frac{\partial \delta^2 l_z}{\partial T} + \frac{1}{\sqrt{-g}} \frac{\partial}{\partial X} (\sqrt{-g} \delta^2 M^X) = 0, \quad (55)$$

where  $\delta^2 l_z = \delta^{1+1} l_z + \delta^{2+0} l_z$ ,  $\delta^2 M^X = \delta^{1+1} M^X + \delta^{2+0} M^X$ ,  $\delta^{1+1} l_z = \delta^{1+1} M^T$ , and  $\delta^{2+0} l_z = \delta^{2+0} M^T$ .

### 3.2. The energy conservation law in the corotating natural frame

We additionally consider the corotating natural coordinates  $(T', X', \Psi', \rho')$  as in Noda et al. (2022),

$$T' = T + \int \frac{IX^2 R^2}{\Gamma \Delta} (\Omega - \Omega_F) dX, \quad (56)$$

$$X' = X, \quad (57)$$

$$\Psi' = \Psi, \quad (58)$$

$$\rho' = \rho - \Omega_F T. \quad (59)$$

The time-like Killing vector of the corotating coordinates is given as  $\xi_{(T')}^{\mu'} = (1, 0, 0, 0)$ , and we have

$$\xi_{(T')}^\mu = \frac{\partial x^\mu}{\partial x^{\nu'}} \xi_{(T')}^{\nu'} = (1, 0, 0, \Omega_F). \quad (60)$$

Then, the 4-vector of the energy flux density in the corotating coordinates is given by

$$S_{(T')}^\mu = -\xi_{(T')}^\nu T_\nu^\mu = S^\mu - \Omega_F M^\mu. \quad (61)$$

The conservation law of the Alfvén wave for (1+1)-order perturbations is

$$\nabla_\mu \delta^{1+1} S_{(T')}^\mu = \frac{1}{\sqrt{-g}} \partial_\mu (\sqrt{-g} \delta^{1+1} S_{(T')}^\mu) = \delta^{1+1} (\xi_{(T')}^\mu f_\mu). \quad (62)$$



The right-hand side of Eq. (62) vanishes because

$$\delta^{1+1}(\xi_{(T')}^\mu f_\mu) = \delta^{1+1}f_T + \Omega_F \delta^{1+1}f_\rho = \frac{1}{\sqrt{-g}}[\partial_\nu(-Z^{\nu\lambda}\partial_\lambda\psi)](\partial_T\psi + \Omega_F\partial_\rho\psi) = 0. \quad (63)$$

Eventually, we obtain the energy conservation law with respect to the Alfvén wave in the corotating magnetic natural frame:

$$\begin{aligned} & \frac{1}{\sqrt{-g}}\partial_\mu(\sqrt{-g}\delta^{1+1}S_{(T')}^\mu) = \frac{1}{\sqrt{-g}}\partial_\mu(\sqrt{-g}(\delta^{1+1}S^\mu - \Omega_F\delta^{1+1}M^\mu)) \\ &= \frac{\partial}{\partial T}(\delta^{1+1}S^T - \Omega_F\delta^{1+1}M^T) + \frac{1}{\sqrt{-g}}\frac{\partial}{\partial X}[\sqrt{-g}(\delta^{1+1}S^X - \Omega_F\delta^{1+1}M^X)] \\ &+ \frac{1}{\sqrt{-g}}\frac{\partial}{\partial\Psi}[\sqrt{-g}(\delta^{1+1}S^X - \Omega_F\delta^{1+1}M^\Psi)] \\ &= \frac{\partial}{\partial T}\left(\delta^{1+1}S^T - \Omega_F\delta^{1+1}M^T + \frac{1}{2}Z^{\Psi\Psi}\psi^2\right) + \frac{1}{\sqrt{-g}}\frac{\partial}{\partial X}[\sqrt{-g}(\delta^{1+1}S^X - \Omega_F\delta^{1+1}M^X)] \\ &= \frac{1}{\sqrt{-g}}\left\{\frac{\partial}{\partial T}\left[\frac{\lambda}{2}\left(\frac{\partial\psi}{\partial T}\right)^2 + \frac{S}{2}\left(\frac{\partial\psi}{\partial X}\right)^2 + \frac{K}{2}\psi^2\right] + \frac{\partial}{\partial X}\left[-S\frac{\partial\psi}{\partial X}\frac{\partial\psi}{\partial T} + V\left(\frac{\partial\psi}{\partial T}\right)^2\right]\right\} = 0. \quad (64) \end{aligned}$$

We write the energy conservation law simply as

$$\frac{\partial}{\partial T}\delta^2e^{\infty'} + \frac{1}{\sqrt{-g}}\frac{\partial}{\partial X}(\sqrt{-g}\delta^2S'_P) = 0, \quad (65)$$

where

$$\delta^2e^{\infty'} = \frac{1}{\sqrt{-g}}\left[\frac{\lambda}{2}\left(\frac{\partial\psi}{\partial T}\right)^2 + \frac{S}{2}\left(\frac{\partial\psi}{\partial X}\right)^2 + \frac{K}{2}\psi^2\right], \quad (66)$$

$$\delta^2S'_P = \frac{1}{\sqrt{-g}}\left[-S\frac{\partial\psi}{\partial T}\frac{\partial\psi}{\partial X} + V\left(\frac{\partial\psi}{\partial T}\right)^2\right] \quad (67)$$

are the energy density and energy flux of the Alfvén wave observed by the corotating magnetic natural frame, respectively. Then, in the corotating frame, the law of conservation of energy holds true even only with the Alfvén wave.

For the angular momentum in the corotating frame, we have

$$M_{(\rho')}^\nu = \xi_{(\rho')}^\mu T_\mu^\nu = \xi_{(\rho')}^\rho = T_\rho^\nu = M^\nu, \quad (68)$$

because

$$\xi_{(\rho')}^\mu = \partial_{\rho'} = \frac{\partial x^\mu}{\partial x^{\rho'}}\xi_{(\rho')}^{\nu'} = \frac{\partial x^\mu}{\partial x^{\rho'}} = \left(0, 0, 0, \frac{\partial\rho}{\partial\rho'}\right) = (0, 0, 0, 1). \quad (69)$$

We then find that the angular momentum densities in the corotating frame ( $x^{\mu'}$ ) and the non-rotating frame ( $x^{\mu}$ ) are identical. This means that the angular momentum of the Alfvén wave alone, as described by  $\psi$ , is not conserved even in the corotating frame, while the energy of the Alfvén wave alone is conserved in the corotating frame. To conserve the angular momentum, we have to consider the fast mode described by the second-order perturbation  $\chi$ .

It is noted that Eq. (61) yields

$$\delta^{1+1}e^{\infty} = \delta^{1+1}e^{\infty'} + \Omega_{\text{F}}\delta^{1+1}l^{z'}, \quad (70)$$

where  $\delta^{1+1}e^{\infty} = \delta^{1+1}S^T$ ,  $\delta^{1+1}e^{\infty'} = \delta^{1+1}S_{(T')}^{T'}$ , and  $\delta^{1+1}l^{z'} = \delta^{1+1}M_{(\rho')}^{T'} = \delta^{1+1}M^T$ . Here,  $\Omega_{\text{F}}\delta^{1+1}l^{z'}$  corresponds to the rotational energy and is converted to the energy of the fast mode because  $\delta^{1+1}e^{\infty'}$  is conserved from Eq. (65).

#### 4. NUMERICAL METHOD

To perform 1D numerical simulations of the force-free field using Eqs. (18) and (25), we use the multi-dimensional two-step Lax-Wendroff scheme for  $\mathbf{u} = (\psi, \xi, \zeta, \chi, v, \sigma)$  whose details are provided in Appendix E. Here,  $\xi, \zeta, v$ , and  $\sigma$  are the new variables introduced for the numerical calculation. We utilize the tortoise coordinate  $x = X - 2M + r_{\text{H}} \log(|X - r_{\text{H}}|/(2M - r_{\text{H}}))$  (see the details in Appendix E). In the numerical calculations, we normalize the length using  $M$ . This scheme sometimes causes numerically artificial structures due to the Gibbs phenomena. To avoid such numerical phenomenon, we employ a smooth profile for the initial variables as follows. The initial

condition of an outwardly/inwardly propagating single pulse of a field is given as:

$$\psi(x) \equiv \begin{cases} \left[ 1 - \left| \frac{x - x_0}{w/2} \right|^{2m} \right]^n & \left( x_0 - \frac{w}{2} \leq x \leq x_0 + \frac{w}{2} \right), \\ 0 & \text{(other)} \end{cases},$$

$$\xi(x) = \bar{v}_{\text{ph}}^{\pm}(x)\psi(x), \tag{71}$$

$$\zeta(x) = 0,$$

$$\chi(x) = 0,$$

$$v(x) = 0,$$

$$\sigma(x) = 0,$$

where the plus and minus signs of  $\bar{v}_{\text{ph}}^{\pm}(x) = \frac{dx}{dX}v_{\text{ph}}^{\pm}(x)$  in the equation with respect to  $\xi(x)$  are taken for the outwardly and inwardly propagating waves, respectively, and  $v_{\text{ph}}^{\pm}$  is given by Eq. (A3). Note that  $x_0$  and  $w$  give the center and the width of the pulse of the Alfvén wave and  $m$  and  $n$  are constants of the pulse shape. In this paper, we set  $n = 32$  and  $m = \log(1 - 2^{-1/32})/\log(1 - 2^{-1/4})$ .

As shown in the next section, we have very smooth numerical results without numerically artificial structures. In this paper, we set the width and position of the outwardly and inwardly propagating pulses to be  $w = 0.5$ ,  $x_0 = -1.6$  (outward pulse) and  $w = 3$ ,  $x_0 = 2$  (inward pulse).

At the inner and outer boundaries,  $x = x_{\text{min}}$  and  $x = x_{\text{max}}$ , the free boundary conditions  $\mathbf{u}_0 - \mathbf{u}_1 = \mathbf{0}$ ,  $\mathbf{u}_I - \mathbf{u}_{I-1} = \mathbf{0}$  are used to mimic the radial boundary condition, where  $\mathbf{u}_0$  and  $\mathbf{u}_I$  are the variables at the boundary and  $\mathbf{u}_1$  and  $\mathbf{u}_{I-1}$  are the values in the neighborhood.

## 5. NUMERICAL RESULTS

We performed 1D numerical simulations of Alfvén waves along a stationary magnetic field line with  $\Omega_{\text{F}} = 0.027$  ( $0 < \Omega_{\text{F}} < \Omega_{\text{H}} = 0.0505$ ) and  $\Omega_{\text{F}} = 0.06$  ( $\Omega_{\text{F}} > \Omega_{\text{H}} = 0.0505$ ) at  $\Psi = 0$  around a black hole with spin parameter  $a = 0.2$  using Eqs. (18) and (26) (Table 1). Here, we set  $M$  to unity. In this case, we have the horizon radius  $r_{\text{H}} = 1 + \sqrt{1 - a_*^2} = 1.9798$ . The radii of the inner and outer light surfaces  $r_{\text{LS}}^- = 1.98$  ( $x_{\text{LS}}^- = -3.03$ ) and  $r_{\text{LS}}^+ = 36.0$  ( $x_{\text{LS}}^+ = 48.7$ ) in the case of  $\Omega_{\text{F}} = 0.027$ ,  $r_{\text{LS}}^- = 1.98$  ( $x_{\text{LS}}^- = -57.8$ ) and  $r_{\text{LS}}^+ = 18.7$  ( $x_{\text{LS}}^+ = 30.0$ ) in the case of  $\Omega_{\text{F}} = \Omega_{\text{H}} = 0.0505$  and  $r_{\text{LS}}^- = 1.98$

( $x_{\text{LS}}^- = -6.55$ ) and  $r_{\text{LS}}^+ = 15.6$  ( $x_{\text{LS}}^+ = 26.5$ ) in the case of  $\Omega_{\text{F}} = 0.06$ . The ergosphere is the region inside the static limit surface,  $r \leq r_{\text{ergo}} = 2$ .

The unstable radial ranges of the Alfvén wave discussed in Section 2.4 for the cases with  $\Omega_{\text{F}} = 0.027$  and  $\Omega_{\text{F}} = 0.06$  are  $r > r_{\text{m}} = 76.8$  ( $x > x_{\text{m}} = 91.1$ ) and  $r > r_{\text{m}} = 15.8$  and ( $x > x_{\text{m}} = 26.7$ ), respectively. The numerical calculations in this paper are performed in the stable radial range ( $r < r_{\text{m}}$ ) except for the region  $26.7 = r_{\text{m}} < r < 30$  in the case of  $\Omega_{\text{F}} = 0.06 > \Omega_{\text{H}}$ . In the case of  $\Omega_{\text{F}} > \Omega_{\text{H}}$ , the Alfvén wave does not enter the unstable region as shown in Section 5.2. However, the Alfvén mode is amplified exponentially when the perturbation is added in the unstable region ( $r > r_{\text{m}}$ ). In this paper, we do not perform numerical simulations for the unstable Alfvén mode.

The initial  $\psi$  conditions are given by  $w = 0.5$  and  $x_0 = -1.5$  at  $T = 0$  in the case of an outwardly propagating pulse in background magnetic fields with  $\Omega_{\text{F}} = 0.027$ ,  $\Omega_{\text{F}} = 0.0505$ , and  $\Omega_{\text{F}} = 0.06$ . In the case of an inwardly propagating pulse, we set  $w = 3$ ,  $x_0 = 4$ , and  $\Omega_{\text{F}} = 0.027$  for the initial condition of  $\psi$  at  $T = 0$ . The initial condition of  $\chi$  is given by  $\chi = 0$  in all cases at  $T = 0$ .

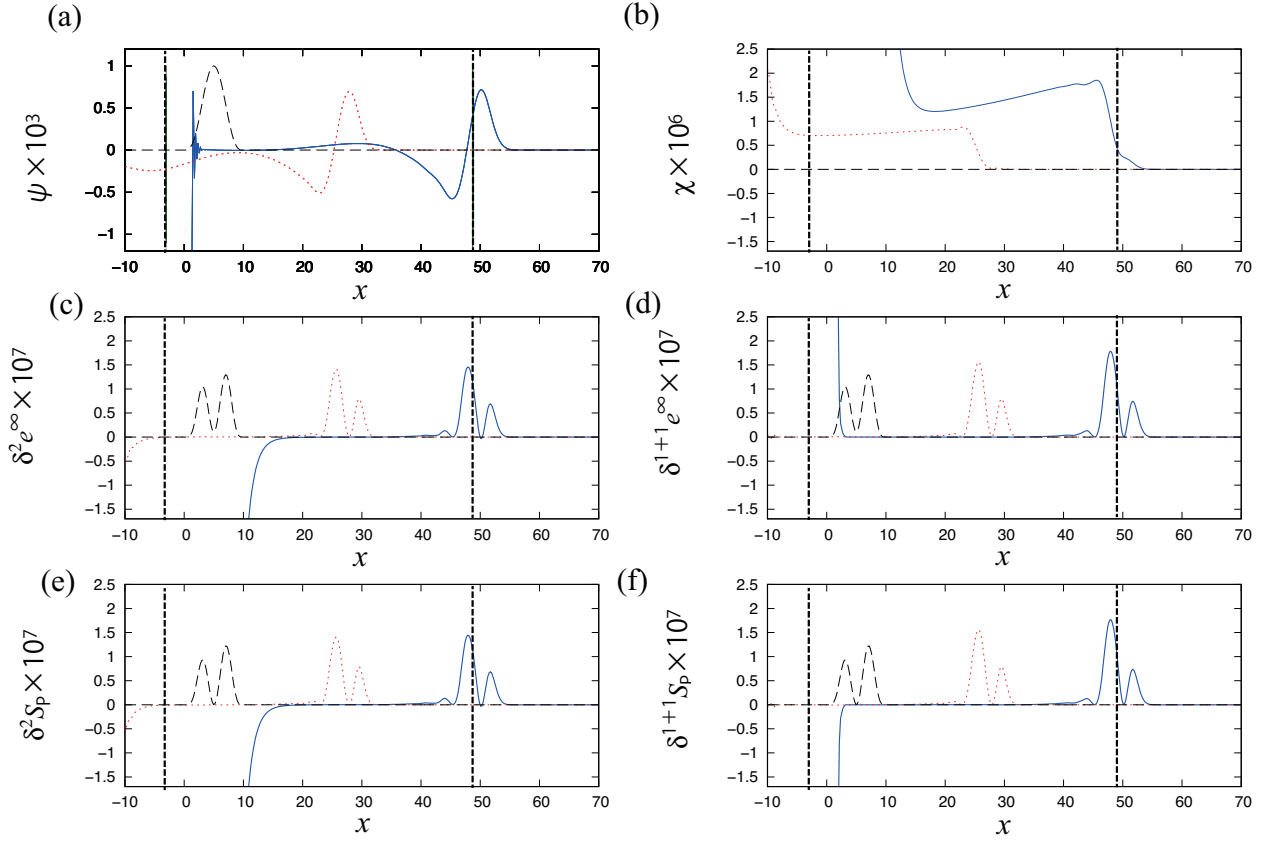
### 5.1. An outwardly propagating Alfvén wave in the case of $\Omega_{\text{F}} < \Omega_{\text{H}}$

Figure 3 shows that the Alfvén wave propagates outward and that the fast wave is caused by the Alfvén wave and propagates toward both the outward and inward sides in the case of  $\Omega_{\text{F}} = 0.027$ ,  $a = 0.2$ ,  $w = 0.5$ , and  $x_0 = -1.5$  (Fig. 3 (a), (b)). The lines in each panel show the results at  $T = 0$  (black dashed line),  $T = 17.5$  (red dotted line), and  $T = 35.0$  (blue, thick solid line) (Fig. 3 (d)). The energy density of the Alfvén wave  $\sqrt{-g}\delta^{1+1}e^\infty$  is initially positive and remains positive, where

| Propagation direction | Relationship between $\Omega_{\text{F}}$ and $\Omega_{\text{H}}$ | $\Omega_{\text{F}}$ | $\Omega_{\text{H}}$ | $a$ | Zeroth order energy flux | $x_0$ | $w$  | Figure number |
|-----------------------|--|---------------------|---------------------|-----|--------------------------|-------|------|---------------|
| Outward               | $0 < \Omega_{\text{F}} < \Omega_{\text{H}}$                      | 0.027               | 0.0505              | 0.2 | $\bar{S}^X > 0$          | 5.0   | 8.0  | 3, 4          |
| Outward               | $\Omega_{\text{F}} \geq \Omega_{\text{H}}$                       | 0.06                | 0.0505              | 0.2 | $\bar{S}^X < 0$          | 5.0   | 8.0  | 5, 6          |
| Inward                | $0 < \Omega_{\text{F}} < \Omega_{\text{H}}$                      | 0.027               | 0.0505              | 0.2 | $\bar{S}^X > 0$          | 20.0  | 20.0 | 8, 9          |

**Table 1.** 1D force-free magnetodynamics (FFMD) simulations of an Alfvén wave along a magnetic field line at the equatorial plane around a Kerr black hole.

the energy density of the Alfvén wave  $\sqrt{-g}\delta^{1+1}e^\infty$  is calculated from only  $\delta^{1+1}e^\infty$  of  $\psi$  without  $\chi$  (see the details in Appendix D). The total energy density of the Alfvén wave and the induced fast wave,  $\sqrt{-g}\delta^2e^\infty$ , remains predominantly positive (Fig. 3 (c)). The integrated energy over the calculation region ( $E(t)$  in Eq. (D54)) is shown in Fig. 4 (i). Here, we calculate the balance with respect to the energy numerically,  $\delta^2\mathfrak{E} = \delta^2E(t) + \delta^2F_1(t) - \delta^2F_2(t)$ , which should be a constant  $\delta^2E(0)$ .  $\delta^{1+1}\mathfrak{E}$  represents the numerical energy balance for the Alfvén wave and  $\delta^{1+1}\mathfrak{E}'$  represents the numerical energy balance for the Alfvén wave in the corotating natural frame. The total energy balance of the Alfvén wave and the induced wave remains constant, which means it is conserved. The induction of the fast wave by the Alfvén wave is explained by the relativistic mechanism, where the Alfvén wave has the angular momentum as in Section 2.5 (Fig. 2).



**Figure 3.** The time evolution of the variables of a force-free electromagnetic field for an initially outwardly propagating pulse of an Alfvén wave along a magnetic field line with  $\Omega_F = 0.027$  (corresponding to the case of black hole energy extraction by the Blandford–Znajek mechanism,  $0 < \Omega_F < \Omega_H$ ) around a Kerr black hole with spin parameter  $a = 0.2$  at  $T = 0.0$  (black dashed line), 25.0 (red dotted line), 50.0 (blue, thick solid line). The dashed vertical lines indicate the inner and outer light surfaces.

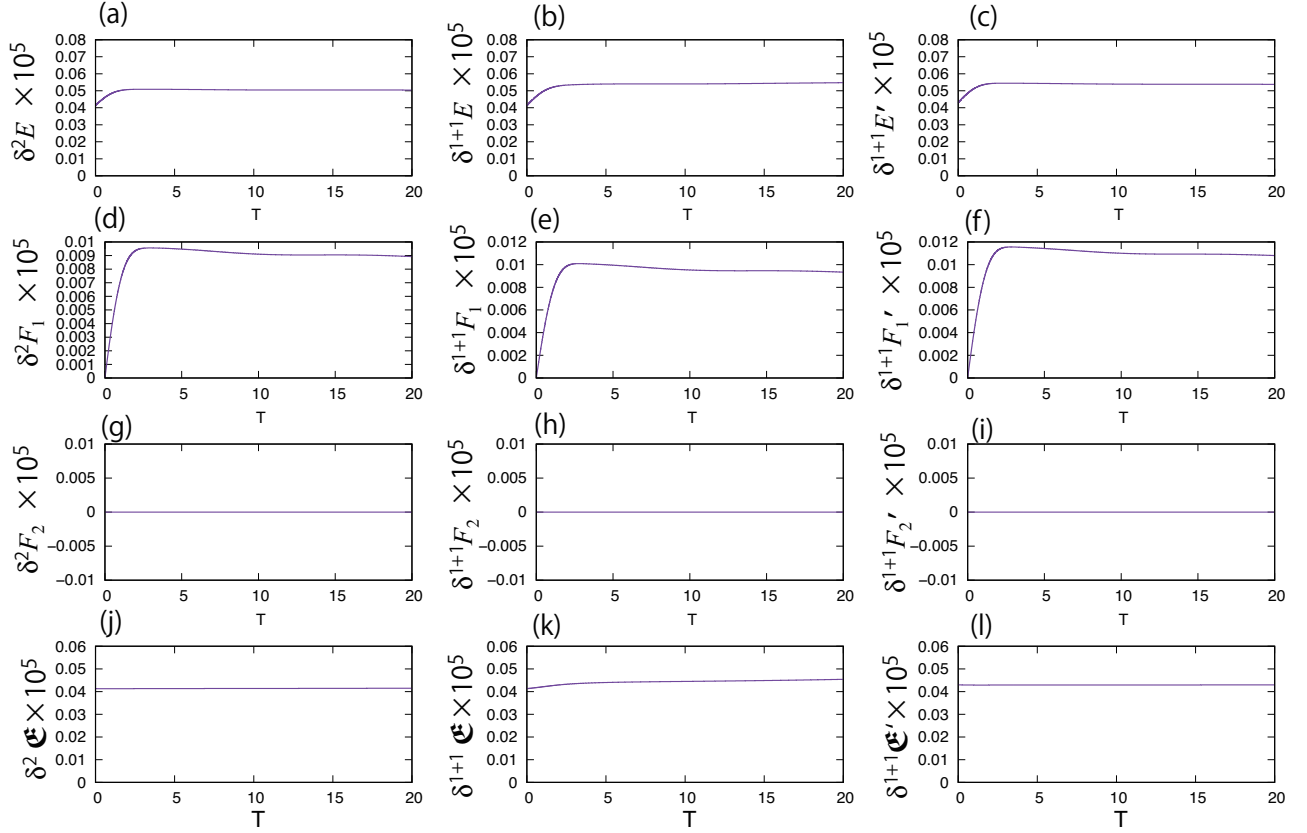


**Figure 4.** The time evolution of the energy balance of the Alfvén and induced fast waves. Top panels: The wave energies. Second panels: The energy fluxes at the left edge. Third panels: The energy fluxes at the right edge. Bottom panels: The balance of energy. Left panels: The Alfvén and fast waves. Middle panels: The Alfvén wave alone. Right panels: The Alfvén wave observed in the corotating frame.

### 5.2. An outwardly propagating Alfvén wave in the case of $\Omega_F > \Omega_H$

As shown in Fig. 5, we also performed a calculation for an Alfvén wave along a magnetic field line with  $\Omega_F = 0.06$ , where the rotational energy of the black hole is not extracted by the Blandford–Znajek mechanism ( $\Omega_F > \Omega_H = 0.0505$ ). The Alfvén wave propagates outward and the fast wave is induced. The induced wave propagates toward both sides as the case of  $\Omega_F = 0.027$  (where the Blandford–Znajek mechanism extracts the black hole rotational energy). The width of the pulse of the Alfvén wave decreases until it vanishes and cannot pass outward through the outer light surface

( $X = r_{\text{LS}+} = 18.7, x = x_{\text{LS}+} = 30.0$ ). Meanwhile, the fast wave induced by the Alfvén wave passes through the outer light surface smoothly.

The slowing of the Alfvén wave near the outer light surface is explained by the dispersion relation of the Alfvén wave provided in Appendix A. This slowing originates from the shape of the magnetic field line (see Fig. 7). The azimuthal component of the magnetic field in the Boyer–Lindquist coordinates is given by  $\bar{B}^\phi = {}^* \bar{F}^{t\phi} = -\frac{I}{\Delta} = -\frac{2M}{\Delta r_{\text{H}}}(\Omega_{\text{H}} - \Omega_{\text{F}})$ , while the radial component of the magnetic field is given by  $\bar{B}^r = {}^* \bar{F}^{tr} = \frac{1}{\Sigma} > 0$  in the equatorial plane ( $\theta = \frac{\pi}{2}$ ). When  $0 < \Omega_{\text{F}} < \Omega_{\text{H}}$ , the magnetic field line bends in the opposite direction to the rotation of the magnetic field line outward, and the azimuthal component of the velocity of the Alfvén wave never exceeds the speed of light (Fig. 7(a)). Otherwise, the magnetic field line bends in the opposite direction, and the wave velocity exceeds the speed of light if it passes over the outer light surface (Fig. 7(b)). Such a situation never occurs, and then the Alfvén wave slows down to stop before the outer light surface, as confirmed by the numerical simulation shown in Fig. 5.



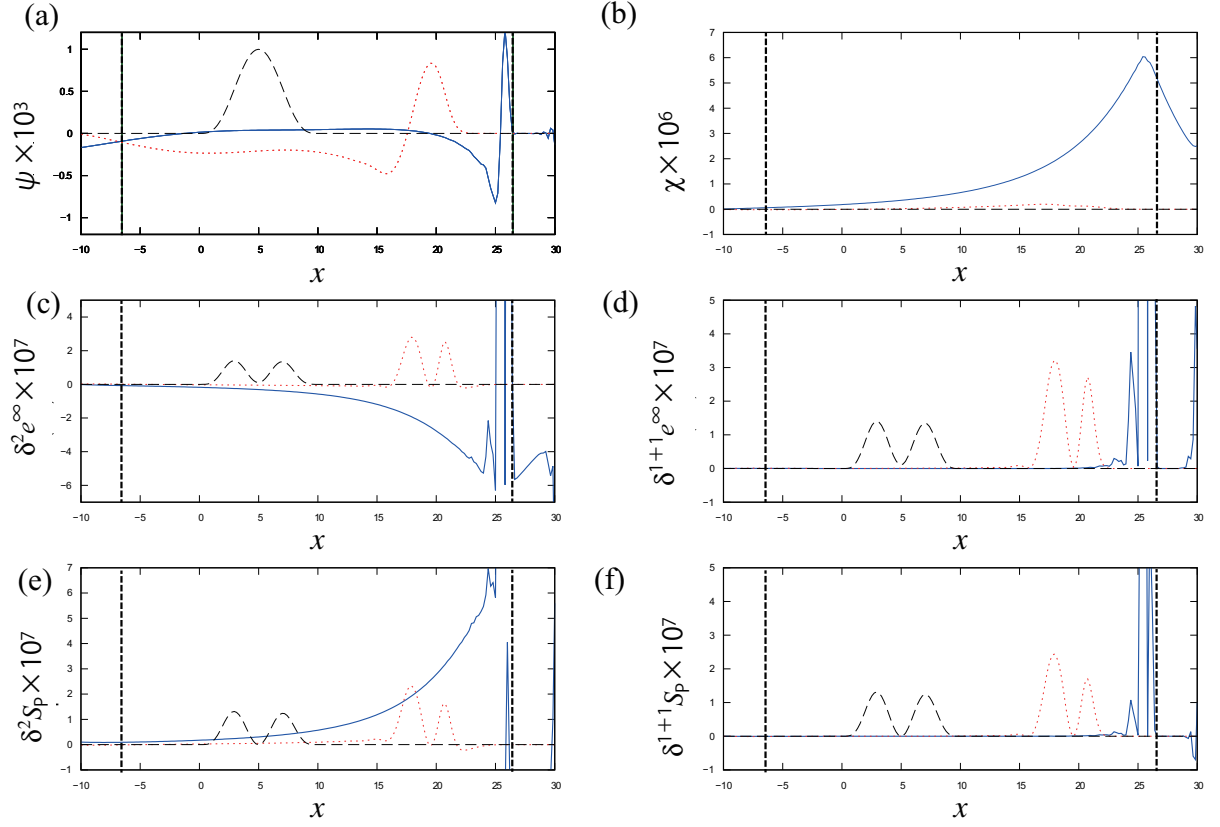


**Figure 5.** Similar to Fig. 3, but for the case of an initially outwardly propagating pulse with a background magnetic field  $\Omega_F = 0.06$  ( $\Omega_F > \Omega_H$ : corresponding to the case with no outward power from the Blandford–Znajek mechanism) at  $T = 0.0$  (black dashed line), 20.0 (red dotted line), 40.0 (blue, thick solid line).

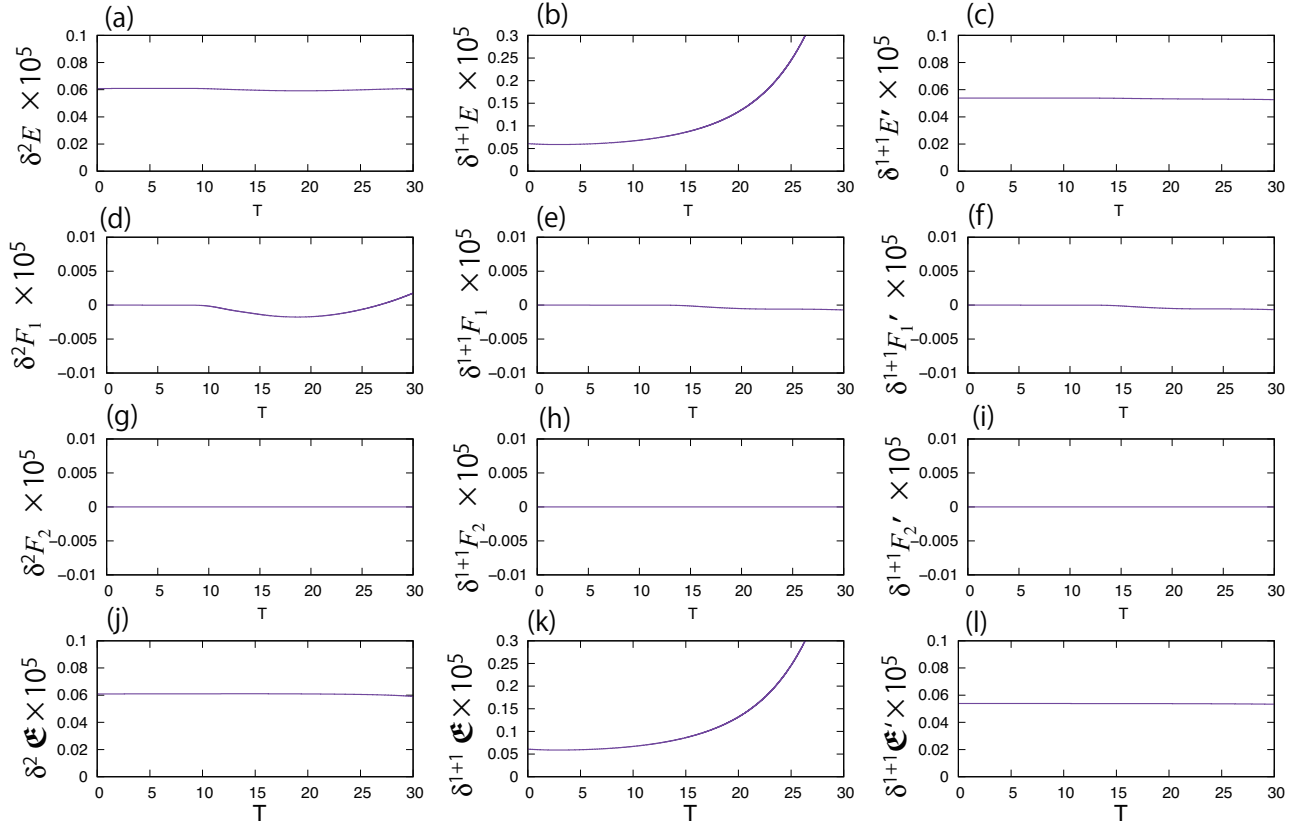


**Figure 6.** Similar to Fig. 4, but for the case of an initially outwardly propagating pulse with the background magnetic field  $\Omega_F = 0.06$  ( $\Omega_F > \Omega_H$ ).

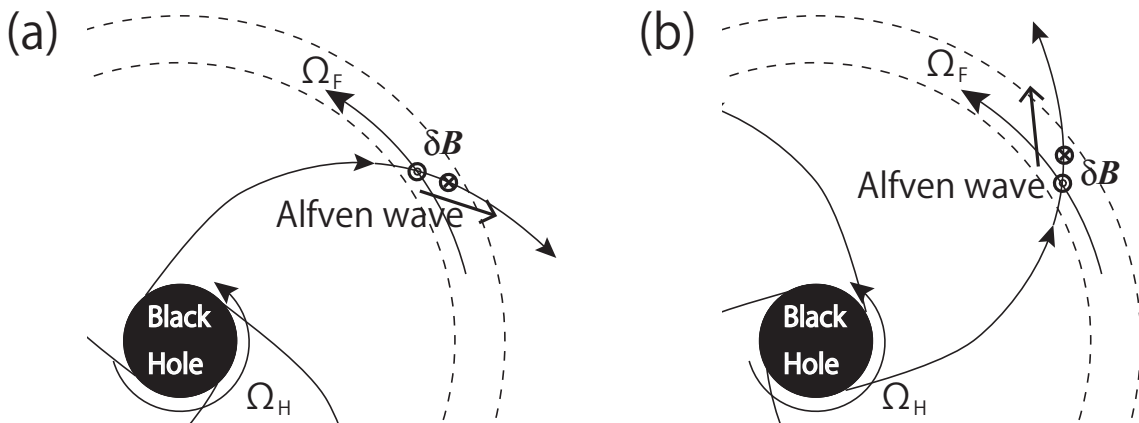
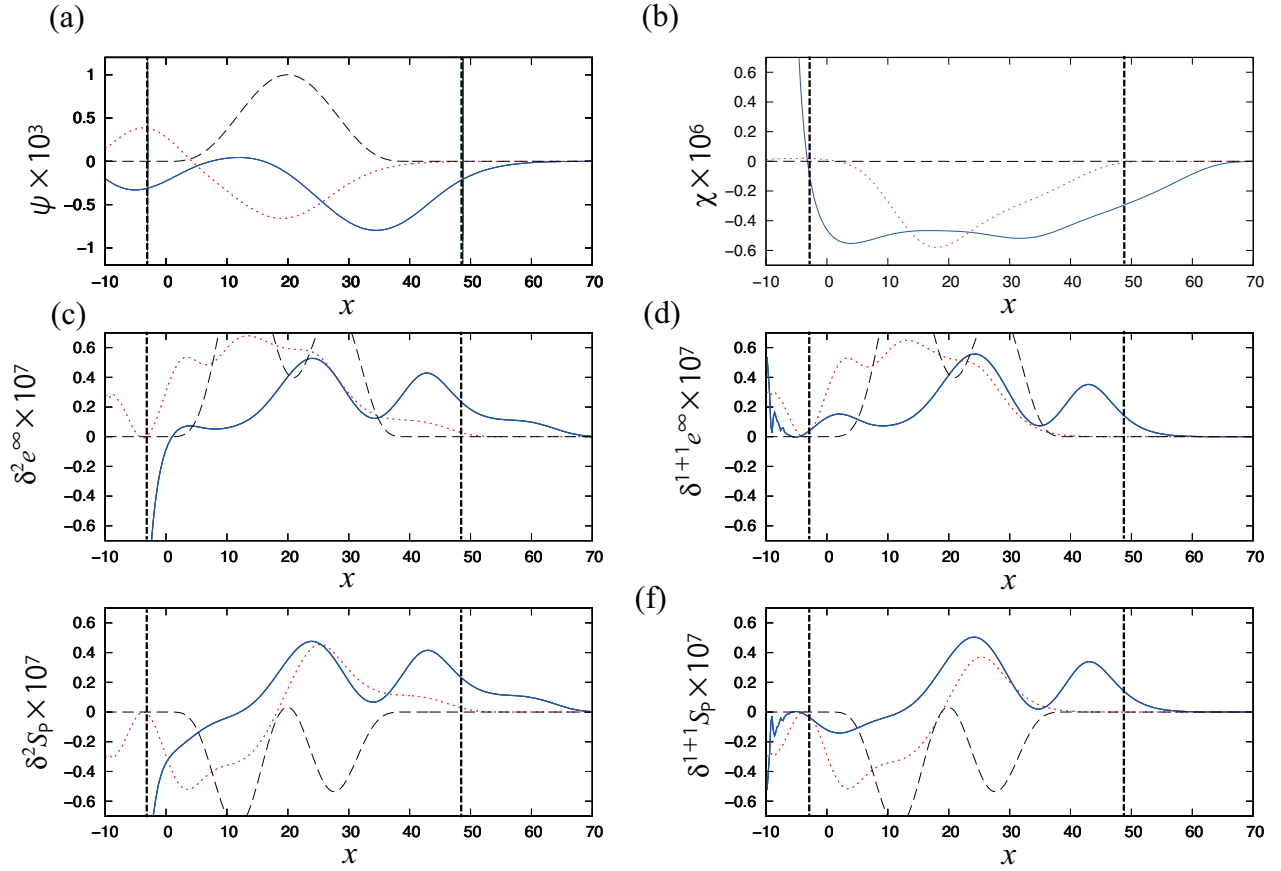


**Figure 7.** A schematic of Alfvén wave pulse propagation along the field line of a force-free magnetic field around a spinning black hole (a) in the case of  $0 < \Omega_F < \Omega_H$  and (b) in the case of  $\Omega_F \geq \Omega_H$ .

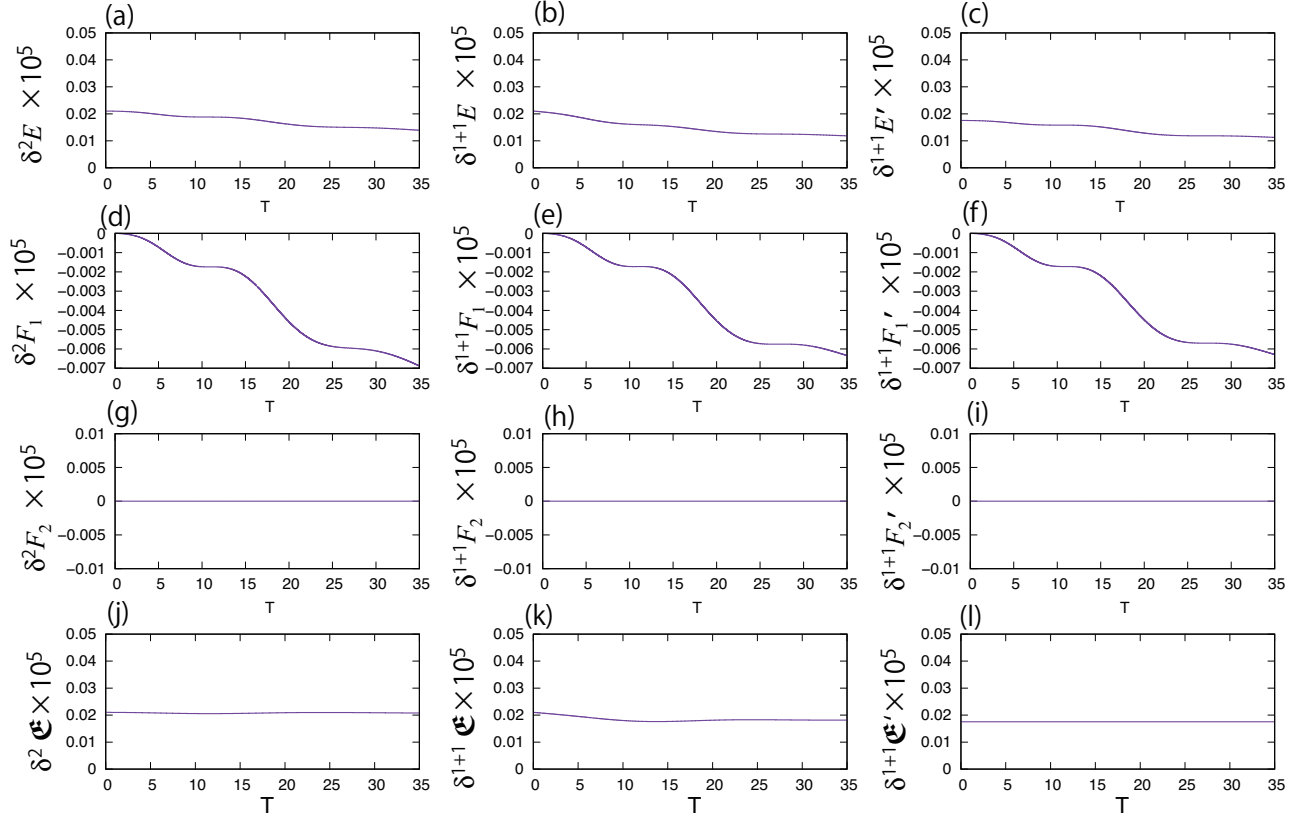
### 5.3. *An inwardly propagating Alfvén wave*

Figure 8 shows the numerical result for the inwardly propagating pulse of an Alfvén wave along a magnetic field line with  $\Omega_F = 0.027$  around a spinning black hole with  $a = 0.2$ . The Alfvén wave pulse propagates inward and induces the fast wave. The induced wave propagates mainly inward with the Alfvén wave pulse. The pulse of the Alfvén wave is reflected as described by Noda et al. (2022) around the point  $x = 5$ , and the pulse is separated into two pulses. This reflection can be explained through the analogy of a wave along a string with an inhomogeneous mass line density  $\lambda$ , tension  $S$ , and spring constant  $K$ , as described by Eq. (18). However, the reflection rate of the wave is less than unity and the superradiance is not shown.

The energy contribution of the induced wave is not so large that  $\sqrt{-g}\delta^2 e^\infty$  is almost equal to  $\sqrt{-g}\delta^{1+1} e^\infty$ . In fact, the time evolution of the total energy almost identical to that of the Alfvén wave (Fig. 9). Thus, in the case of an inward-propagating wave from the outer region, the fast induced wave is negligible in the energy conservation law.



**Figure 8.** The time evolution of the variables of a force-free electromagnetic field for an initially inwardly propagating pulse of an Alfvén wave from a region in the ergosphere along a magnetic field line with  $\Omega_F = 0.027$  (corresponding to the case of black hole energy extraction via the Blandford–Znajek mechanism,  $0 < \Omega_F < \Omega_H$ ) around a spinning black hole with spin parameter  $a = 0.2$  at  $T = 0.0$  (black dashed line), 17.5 (red dotted line), 35.0 (blue, thick solid line). The dashed-dotted lines show the location of the light surfaces. The reflection of the wave is shown around  $x = 5$ .



**Figure 9.** Similar to Fig. 4, but for the case of an initially inwardly propagating pulse with the background magnetic field  $\Omega_F = 0.027$  ( $0 < \Omega_F < \Omega_H$ ).

## 6. CONCLUDING REMARKS

In this work, we have performed 1D linear analysis and numerical simulations of force-free Alfvén waves and induced fast waves along a magnetic field line at the equatorial plane around a black hole in a non-rotating natural coordinate frame using Eq. (18) for  $\psi$  and Eq. (26) for  $\chi$  to satisfy the force-free condition and energy conservation. We identified the following interesting phenomena.

- The Alfvén wave induces a fast magnetosonic wave when its angular momentum changes due to the rotation and bending of the background magnetic field lines. The total energy and angular momentum of the Alfvén wave and the fast wave are conserved, while the energy and angular momentum of the Alfvén wave alone are not conserved.

- In the case of  $\Omega_F > \Omega_H$ , the outwardly propagating Alfvén wave never passes through the outer light surface, while in the case of  $\Omega_F < \Omega_H$ , it passes through the outer light surface smoothly. The fast wave passes through the outer light surface in any case.
- The inwardly propagating Alfvén wave is reflected around the region near the inner light surface. Within the numerical calculations, we found no phenomenon suggesting superradiance of the reflected Alfvén wave.
- The Alfvén wave is unstable over the region  $r = X > r_m$ , where  $r_m$  is the solution for  $K = 0$  outside the outer light surface when  $\Omega_F > \Omega_c = \frac{2M}{2M + r_H} |\Omega_H|$ . When  $\Omega_F < \Omega_c$ , the Alfvén wave propagates stably.

The fast wave induced by the Alfvén wave is attributed to a change in the angular momentum of the Alfvén wave (Fig. 2). The Alfvén wave has momentum and angular momentum in the relativistic framework.<sup>5</sup> When the Alfvén wave propagates along a curved magnetic field line, the angular momentum changes due to the torque from the background magnetic field. The reaction of the torque induces the fast wave described by  $\chi$ . The above mechanism is expected to work in the relativistic magnetohydrodynamic (MHD) framework. Therefore, in a non-relativistic MHD framework, the angular momentum of the Alfvén wave vanishes, and the fast wave is not induced. The second-order fast wave is induced by the Alfvén wave only in relativistic MHD. This mechanism explains the conversion of the Alfvén wave into a fast magnetosonic wave in the pulsar magnetosphere, as shown by Yuan et al. (2021). The authors showed that an Alfvén wave loses energy due to induction of the fast mode. The same energy conversion of the Alfvén wave is found in the case with  $\Omega_F = 0.06 > \Omega_H$  (Fig. 6). However, in the case with  $\Omega_F = 0.027 < \Omega_H$ , the energy of the Alfvén wave pulse increases as it propagates outward from the ergosphere (Fig. 4).

In the case of outward power radiation via the Blandford–Znajek mechanism ( $0 < \Omega_F < \Omega_H$ ), the outwardly propagating Alfvén wave pulse passes through the outer light surface smoothly. In the

<sup>5</sup> In the special relativistic framework, the momentum density of the transverse wave is given by  $\vec{S}/c^2$ , where  $\vec{S}$  is the Poynting flux and  $c$  is the speed of light. In the nonrelativistic limit ( $c \rightarrow \infty$ ), the momentum density vanishes.

case without this stationary outward power radiation ( $\Omega_F > \Omega_H$ ), the pulse of the Alfvén wave never passes the outer light surface, while the induced fast waves pass smoothly through. This is because the speed of the Alfvén wave along the magnetic field line exceeds the speed of light when the outward Alfvén wave has passed through the outer light surface because the magnetic field line is oblique with  $B^\phi/B^r > 0$  in the case of  $\Omega_F > \Omega_H$  (see Fig. 7(b)).

The Alfvén wave is unstable in the region outside the outer light surface, while the Alfvén wave is stable over the whole region in the case of  $\Omega_F < \Omega_c = \frac{2M}{2M + r_H} |\Omega_H|$ . The instability of the Alfvén wave may explain the winding of the magnetic surface around the equatorial plane near the Kerr black hole, as shown in recent GRMHD simulations (Ripperda et al. 2022).

In this paper, we have used the stationary background solution in precisely the same way as Noda et al. (2020) and we found that the Alfvén wave is reflected near the inner light surface but we did not identify the superradiance phenomenon. This may be due to the initial perturbation conditions of the Alfvén wave.

## ACKNOWLEDGMENTS

We are grateful to Mika Inda-Koide and Yasusada Nambu for their helpful comments on this paper. S.N. was supported by JSPS KAKENHI Grant No. 24K17053.

## REFERENCES

- Acciari, V. A., Aliu, E., Arlen, T., et al. 2009, *Sci*, 325, 444.
- Antolin, P., Shibata, K., Kudoh, T., Shiota, D., & Brooks, D. 2008, *ApJ*, **688**, 669.
- Banados, M., Teitelboim, C., & Zanelli, J. 1992, *PhRvL*, **69**, 1849.
- Bellman, P. M. 2006, *Fundamentals of Plasma Physics* (Cambridge University Press, Cambridge)
- Biretta, J. A., Sparks, W. B., & Macchetto, F. 1999, *ApJ*, **520**, 621
- Blandford, R. D. & Znajek, R. 1977, *MNRAS*, **179**, 433

- Event Horizon Telescope Collaboration 2019, *ApJL*, 875, L5.
- Gammie, C. F., McKinney, J. C., & Toth, G. 2003, *ApJ*, **589**, 444.
- Gravity Collaboration 2017, *A&A*, 602, A94.
- Hakobyan H., Ripperda B., & Philippov A. 2023, *ApJ*, 943, L29.
- Jacobson, T. & Rodriguez, M. J. 2019, *PhRvD*, **99**, 124013.
- Kathirgamaraju, A., Tchekhovskoy, A., Giannios, D., & Duran, R. B. 2019, *MNRAS*, **484**, L98.
- Koide, S. 2003, *PhRvD*, **67**, 104010.
- Koide, S. 2004, *ApJL*, **606**, L45.
- Koide, S. , Kudoh, T., Shibata, K. 2006, *PhRvD*, **74**, 044005
- Koide, S. Noda, S., Takahashi, M., & Nambu, Y. 2022, *ApJ*, **928**, 84.
- Komissarov, S. S. 2004, *MNRAS*, **350**, 1431.
- Komissarov, S. S. 2005, *MNRAS*, **359**, 801.
- McKinney, J. C. 2006, *MNRAS*, **368**, 1561
- McKinney, J. C. & Blandford, R. D. 2009, *MNRAS*, **394**, L126
- Mizuno, Y., Yamada, S., Koide, S., & Shibata, K. 2004, *ApJ*, **615**, 389.
- Musielak, Z. E., Routh, S. & Hammer, R. 2007, *ApJ*, **659**, 650.
- Nagataki, S. 2009, *ApJ*, **704**, 937.
- Nathanail A., Fromm C. M., Porth O., Olivares H., Yousni Z., Mizuno Y., & Rezzolla L., 2020, *MNRAS*, 495, 1549.
- Noda, S., Nambu, Y., Tsukamoto, T., & Takahashi, M., 2020, *PhRvD*, 101, 023003.
- Noda, S., Nambu, Y., Tsukamoto, T., & Takahashi, M., 2022, *PhRvD*, 105, 064018.
- Paschalidis, V., Ruiz, M., & Shapiro, S. L. 2015, *ApJ*, **806**, L14.
- Pearson, T. J. et al. 1981, *Nature*, 290, 365.
- Porth, O., Chatterjee, K., Narayan, R. et al. 2019, *ApJS*, **243**, id. 26.
- Press, W. H., & Teukolsky, S. A., *Nature*, **238**, 211 (1972).
- Teukolsky, S. A., & Press, W. H., *ApJ*, **193**, 443 (1974).
- Ripperda, B., Bacchini, F. & Philippov, A. A. 2020, *ApJ*, 900, 100.
- Ripperda, B., Liska, M., Chatterjee, K., Musoke, G., Philippov, A. A., Markoff, S. B., Tchekhovskoy, A., & Younsi, Z. 2022, *ApJ*, **924**, L32.
- Ruiz, M., Lang, R. N., Paschalidis, V., & Shapiro, S. L. 2016, *ApJ*, **824**, L6.
- Uchida, T. 1997a, *Monthly Notices of the Royal Astronomical Society*, **286**, 931.
- Uchida, T. 1997b, *Monthly Notices of the Royal Astronomical Society*, **291**, 125.
- Yuan, Y., Levin, Y., Bransgrove, A., & Philippov, A. 2021, *ApJ*, **908**, id. 176 (12pp).



## APPENDIX

## A. THE DISPERSION RELATION OF AN ALFVÉN WAVE AROUND A SPINNING BLACK HOLE

In this appendix, we discuss the strange behavior of an Alfvén wave propagating along a magnetic field line using the eikonal approximation. The dispersion relation of the wave governed by Eq. (18) is given by

$$\omega = \frac{V \pm \sqrt{V^2 + \lambda S}}{\lambda} k = \frac{V \pm \sqrt{\Sigma K} / \sin \theta}{\lambda} k \quad (\text{A1})$$

in the small wavelength limit. The dispersion relation shows that when  $K$  is negative, the Alfvén wave is unstable. Hereafter, we consider a perturbation on the equatorial surface  $\theta = 90^\circ$  ( $\Psi = 0$ ). At the infinity point ( $X \rightarrow \infty$ ), we have

$$K = \frac{\alpha^2 - R^2(\Omega_F - \Omega)^2 + I^2 X^2}{\Delta} \rightarrow \frac{X^2}{\Delta} \left[ \frac{2M}{r_H} \Omega_H - \left( \frac{2M}{r_H - M} \right) \Omega_F \right] \left[ \frac{2M}{r_H} \Omega_H - \left( \frac{2M}{r_H + M} \right) \Omega_F \right]. \quad (\text{A2})$$

Then, in the case of  $\Omega_c \equiv \frac{2M}{2M + r_H} |\Omega_H| < |\Omega_F| < \frac{2M}{2M - r_H} |\Omega_H|$ ,  $K$  becomes negative at a point far enough from the black hole ( $r \gg r_H$ ); that is, the Alfvén wave in an outer region far enough from the hole is unstable. In Fig. 10, we plot  $K$  with respect to the position  $x$  and  $\Omega_F$  in the case of the spin parameter  $a = 0.2$ . For the case of  $\Omega_F = 0.02$ , the Alfvén wave propagates stably in the range  $x \leq 120$ , while for  $\Omega_F = 0.027$  the Alfvén wave becomes unstable at  $x > 91.1$ .

It is noted that an Alfvén wave around a Schwarzschild black hole is always stable because  $\Omega_H = 0$  and the unstable condition of the wave can never be satisfied. Figure 11 shows the contour of  $K = 0$  at  $X = r_m$  for the case of  $0 \leq a \leq 1$  and  $0 \leq |\Omega_F| \leq 0.5$ .  $r_m$  is the marginal radial coordinate of the instability of the Alfvén wave, where  $r_m$  is the solution for  $K = 0$ . The Alfvén wave is unstable at  $X > r_m$  and stable at  $X < r_m$ . The line of  $\Omega_F = \Omega_H$  in Fig. 11 shows that the Alfvén wave is always unstable in the case of  $\Omega_F = \Omega_H$ , which is surprising, while the wave is stable in the case of  $\Omega_F = \Omega_H/2$  because  $\Omega_H/2 < \frac{2M}{2M + r_H} |\Omega_H| \equiv \Omega_c$ . For example, in the case of  $a_* = a/M = 0.2$  and  $\Omega_F = \Omega_H$ , the Alfvén wave is unstable in the region of  $X > 9.5r_H = 18.8M$ . However, the contours of

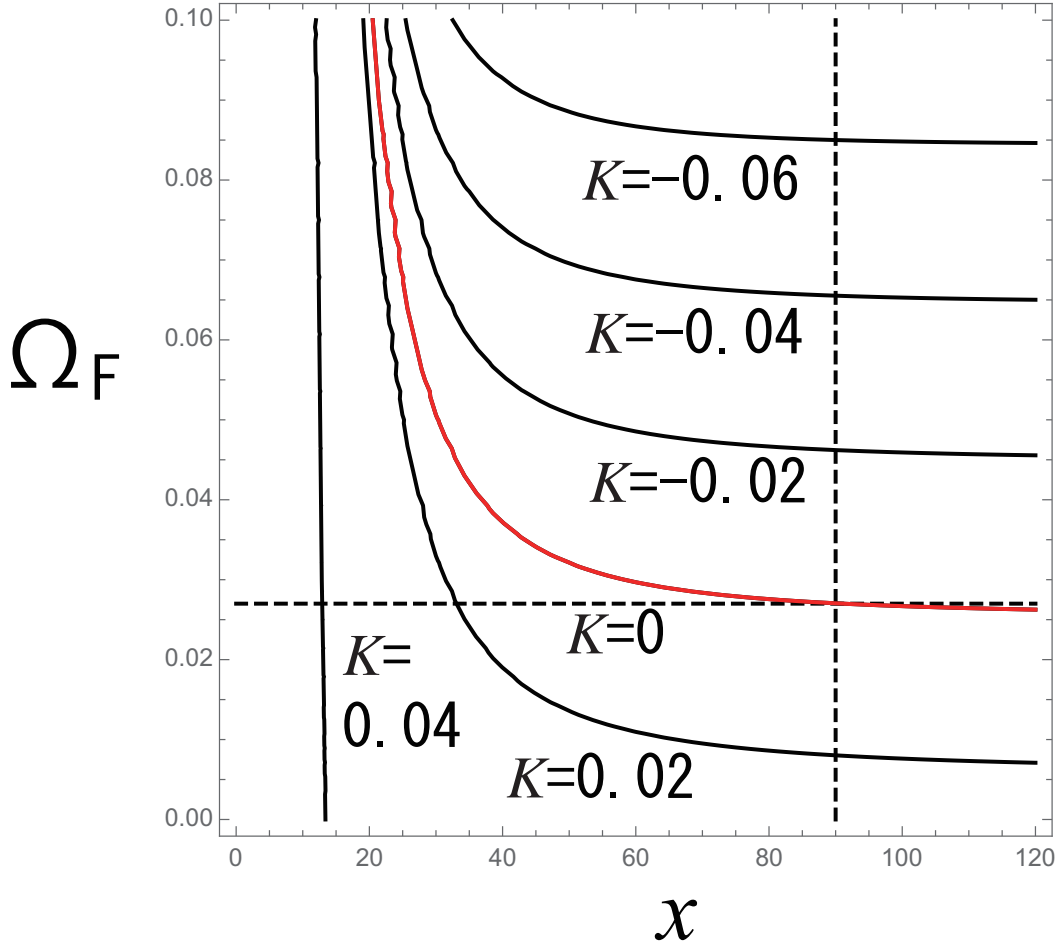


**Figure 10.** The propagation diagram of the Alfvén wave with the plot of  $K$  in the case of the spin parameter  $a = 0.2$ . The solid red line shows the line of  $K = 0$ . When  $K$  is negative the propagation of the Alfvén wave is unstable, while the wave propagation is stable when  $K$  is positive. The horizontal dashed line:  $\Omega_F = 0.027$ . The vertical dashed line:  $x = 91$ .

$K = 0$  confirm that the Alfvén wave is stable when  $\Omega_F < \frac{2M}{2M + r_H} |\Omega_H| \equiv \Omega_c$ . Hereafter, we mainly consider the propagating Alfvén wave in the stable region  $X < r_m$  or in the case of  $\Omega_F \geq \Omega_c$ .

The dispersion relation (A1) shows that the velocity of an Alfvén wave governed by Eq. (18) is

$$v_{\text{ph}}^{\pm} = \frac{\omega}{k} = \frac{V \pm \sqrt{V^2 + \lambda S}}{\lambda} = \frac{V \pm \sqrt{\Sigma K} / \sin \theta}{\lambda} \quad (\text{A3})$$

when the wavelength is small enough. Note also that Eq. (A3) shows the propagation directions of the waves with  $v_+$  and  $v_-$  are the same when  $S$  is negative or equal to zero. Between the outer and inner light surfaces,  $S$  is positive. However, outside of the region between the two light surfaces,  $S$

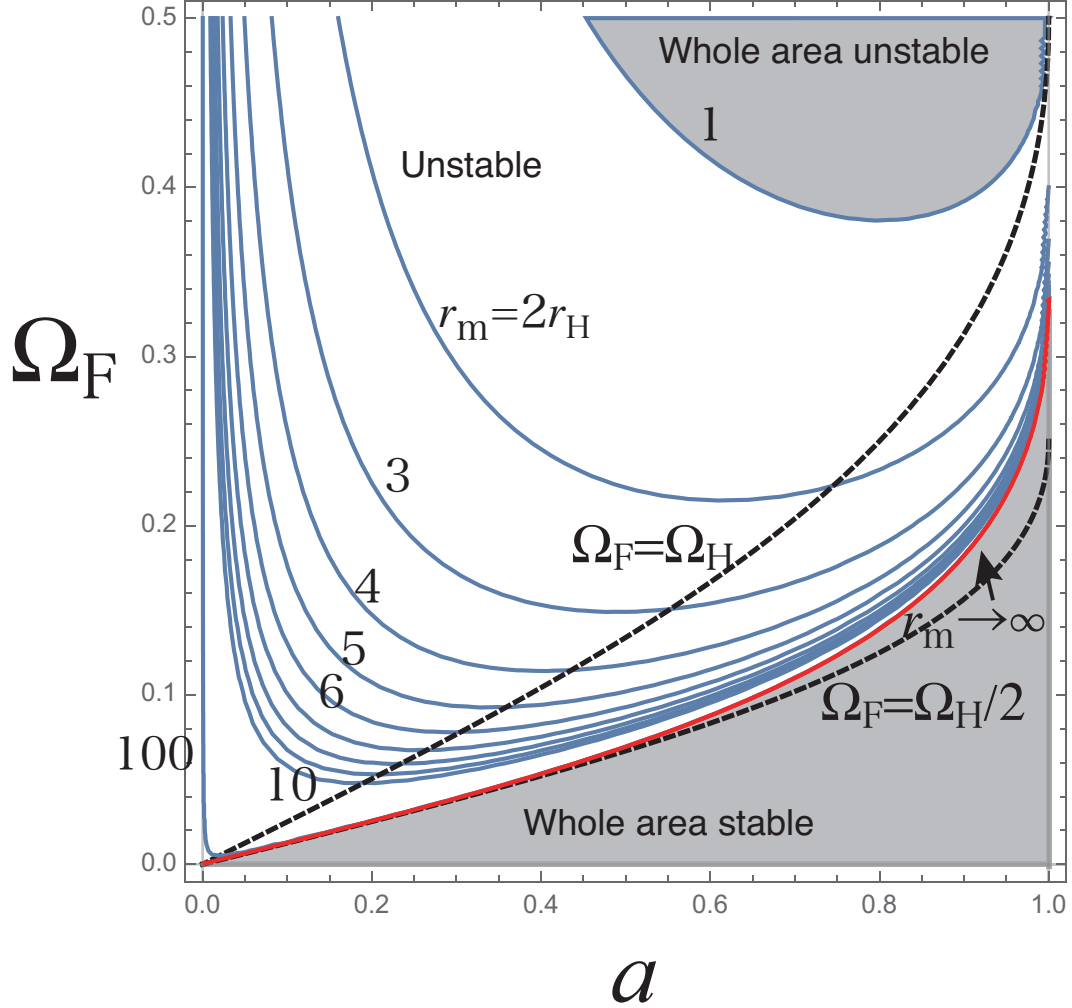


**Figure 11.** The unstable region of Alfvén wave propagation on the equatorial plane for each  $a$  and  $\Omega_F$ . The Alfvén wave at  $X > r_m$  ( $r > r_m$ ) is unstable. When  $\Omega_F$  is below the line of  $r_m \rightarrow \infty$ , the Alfvén wave is stable throughout the region from the horizon to infinity.

is negative. Thus, we conclude that the Alfvén wave propagates only in one direction outside the region between the inner and outer light surfaces. This conclusion is also significant.

Here, we consider the head velocity of an outwardly propagating Alfvén wave at the outer light surface, which is given by

$$v_{h,LS+} = \lim_{k \rightarrow \infty} \frac{\omega}{k} = v_{ph}^+(r_{LS}^+) = \frac{V + |V|}{\lambda}, \quad (\text{A4})$$

because  $S$  vanishes at the light surface. The head velocity represents the upper limit of the propagation velocity of information. When  $0 < \Omega_F < \Omega_H$ , the head velocity of the Alfvén wave at the

outer light surface,  $v_{\text{h,LS}+}$  becomes  $\frac{2V}{\lambda}$  because  $V$  is positive. Meanwhile, when  $\Omega_{\text{F}} < 0$  or  $\Omega_{\text{F}} > \Omega_{\text{H}}$ ,  $v_{\text{h,LS}+}$  vanishes because  $V$  is negative. This means the Alfvén wave never passes through the outer light surface outward when  $\Omega_{\text{F}} < 0$  or  $\Omega_{\text{F}} > \Omega_{\text{H}}$ , while it does when  $0 < \Omega_{\text{F}} < \Omega_{\text{H}}$ . This results from the shape of the magnetic field line (Fig. 7). The azimuthal component of the magnetic field in Boyer–Lindquist coordinates is given by  $\bar{B}^\phi = {}^* \bar{F}^{t\phi} = -\frac{I}{\Delta} = -\frac{2M}{\Delta r_{\text{H}}}(\Omega_{\text{H}} - \Omega_{\text{F}})$ , while the radial component of the magnetic field is given by  $\bar{B}^r = {}^* \bar{F}^{tr} = \frac{1}{\Sigma} > 0$  at the equatorial plane  $\theta = \frac{\pi}{2}$ . When  $0 < \Omega_{\text{F}} < \Omega_{\text{H}}$ , the magnetic field line bends in the opposite direction to the rotation of the magnetic field line outward, and the azimuthal component of the velocity of the Alfvén wave never exceeds the speed of light. Otherwise, the magnetic field line bends in the opposite direction, and the wave velocity exceeds the speed of light if it passes over the outer light surface.

## B. THE ENERGY-MOMENTUM TENSOR AND FORCE-FREE CONDITION FOR AN ALFVÉN WAVE

We show the detailed calculation with respect to the energy-momentum tensor and the force-free condition in the case of the Alfvén wave only, where we assume

$$\phi_1 = \bar{\phi}_1 + \delta\phi_1 = -\cos\theta + \psi, \quad \phi_2 = \bar{\phi}_2. \quad (\text{B5})$$

First, we show non-zero components of the field tensor of the equilibrium, first and second-order perturbations as follows. Non-vanishing components of the field tensor of the equilibrium are only

$$\bar{F}_{\rho\Psi} = -\bar{F}_{\Psi\rho} = -1, \quad \bar{F}^{\mu\Psi} = -\bar{F}^{\Psi\mu} = Y^{\mu\Psi\Psi} \quad (\mu \neq \Psi). \quad (\text{B6})$$

The field tensor of the first-order perturbations are

$$\delta F_{\mu\nu} = -\delta F_{\nu\mu} = (\delta_\nu^\rho - \Omega_{\text{F}}\delta_\nu^T)\partial_\mu\psi - (\delta_\mu^\rho - \Omega_{\text{F}}\delta_\mu^T)\partial_\nu\psi \quad (\lambda \neq \rho), \quad \delta F^{\mu\nu} = Y^{\mu\lambda\nu}\partial_\lambda\psi. \quad (\text{B7})$$

All components of the field tensor of the second-order perturbations vanish.

Then, we calculate

$$\bar{F}^{\mu\lambda}\delta F_{\nu\lambda} = \bar{F}^{\mu\Psi}\delta F_{\nu\Psi} = g^{\mu\rho}\delta F_{\nu\Psi} = 0, \quad (\text{B8})$$

$$\bar{F}^{\lambda\kappa}\delta F_{\lambda\kappa} = \bar{F}_{\lambda\kappa}\delta F^{\lambda\kappa} = 2\bar{F}_{\rho\Psi}\delta F^{\rho\Psi} = 2W^{\rho\lambda\Psi\rho}\partial_\lambda\psi = -2g^{\rho\rho}g^{\lambda\Psi}\partial_\lambda\psi = 0. \quad (\text{B9})$$

We find

$$\begin{aligned}\delta F^{\mu\lambda}\bar{F}_{\nu\lambda} &= \delta F^{\mu\Psi}\bar{F}_{\nu\Psi} + \delta F^{\mu\rho}\bar{F}_{\nu\rho} = \delta F^{\nu\Psi}\delta_{\nu\rho} - \delta^{\mu\rho}\delta_{\nu\Psi} = W^{\mu\lambda\Psi\rho}\partial_\lambda\psi\delta_{\nu\rho} - W^{\mu\lambda\rho\rho}\partial_\lambda\psi\delta_{\nu\Psi} \\ &= -g^{\mu\rho}g^{\Psi\Psi}\partial_\Psi\psi\delta_{\nu\rho} - W^{\mu\lambda\rho\rho}\partial_\lambda\psi\delta_{\nu\Psi} = -W^{\mu\lambda\rho\rho}\partial_\lambda\psi\delta_{\nu\Psi} = 0.\end{aligned}\quad (\text{B10})$$

Because when  $\nu = \rho$ , we have  $\delta F_{\rho\Psi} = -\partial_\Psi\psi = 0$ , and otherwise, we have  $\delta F_{\nu\Psi} = 0$ . Then, we conclude that when  $\mu$  and  $\nu$  are not  $\Psi$ , we have

$$\delta T_\nu^\mu = 0. \quad (\text{B11})$$

To check the force-free condition, we calculate the Lorentz force,

$$f_\mu^L = J^\nu F_{\mu\nu}, \quad J^\mu = \nabla_\nu F^{\mu\nu} = \frac{1}{\sqrt{-g}}\partial_\nu(\sqrt{-g}F^{\mu\nu}). \quad (\text{B12})$$

First, we can confirm the Lorentz force of the equilibrium vanishes because the 4-current density of the equilibrium vanishes:

$$\bar{J}^\mu = \frac{1}{\sqrt{-g}}\partial_\nu(\sqrt{-g}\bar{F}^{\mu\nu}) = \frac{1}{\sqrt{-g}}\partial_X(\sqrt{-g}\bar{F}^{\mu X}) = 0, \quad \bar{f}_\mu^L = \bar{J}^\nu \bar{F}_{\mu\nu} = 0, \quad (\text{B13})$$

Second, we confirm the Lorentz force with respect to the first-order perturbation of Alfvén wave vanishes:

$$\delta f_i^L = \delta J^\nu \bar{F}_{i\nu} = 0, \quad (\text{B14})$$

$$\delta f_\rho^L = \delta J^\nu \bar{F}_{\rho\nu} = \delta J^\Psi \bar{F}_{\rho\Psi} = \delta J^\Psi = \frac{1}{\sqrt{-g}}\partial_\nu(\sqrt{-g}\bar{F}^{\Psi\nu}) = \frac{1}{\sqrt{-g}}\partial_\nu(\sqrt{-g}Y^{\Psi\lambda\nu}\partial_\lambda\psi) = 0, \quad (\text{B15})$$

$$\begin{aligned}\delta f_\Psi^L &= \delta J^\nu \bar{F}_{\Psi\nu} = \delta J^\rho \bar{F}_{\Psi\rho} = -\delta J^\rho = -\frac{1}{\sqrt{-g}}\partial_\nu(\sqrt{-g}\delta F^{\rho\nu}) \\ &= -\frac{1}{\sqrt{-g}}\partial_\nu(\sqrt{-g}Y^{\rho\lambda\nu}\partial_\lambda\psi) = \frac{1}{\sqrt{-g}}\partial_\nu(\sqrt{-g}Z^{\nu\lambda}\partial_\lambda\psi) = 0,\end{aligned}\quad (\text{B16})$$

where  $i$  is  $T$  or  $X$ . In the last equation of Eq. (B16), we use Eq. (17). Then, we confirmed the first order of the Lorentz force vanishes.

It is noted that we have  $\delta J^\rho = \delta J^\Psi = 0$ . Using

$$\delta J^\mu = \frac{1}{\sqrt{-g}}\partial_\nu(\sqrt{-g}\delta F^{\mu\nu}) = \frac{1}{\sqrt{-g}}\partial_\nu(\sqrt{-g}Y^{\mu\lambda\nu}\partial_\lambda\psi), \quad (\text{B17})$$

we have

$$\delta J^T = \frac{1}{\sqrt{-g}} \sum_{\lambda=T,X} \partial_\nu(\sqrt{-g}Y^{T\lambda\nu}\partial_\lambda\psi) = \frac{1}{\sqrt{-g}} \sum_{\lambda=T,X} \partial_X(\sqrt{-g}Y^{T\lambda X}\partial_\lambda\psi), \quad (\text{B18})$$

$$\delta J^X = \frac{1}{\sqrt{-g}} \sum_{\lambda=T,X} \partial_\nu(\sqrt{-g}Y^{X\lambda\nu}\partial_\lambda\psi) = -\frac{1}{\sqrt{-g}} \sum_{\lambda=T,X} \partial_X(\sqrt{-g}Y^{T\lambda X}\partial_\lambda\psi), \quad (\text{B19})$$

$$\delta J^\rho = \delta J^\Psi = 0, \quad (\text{B20})$$

where  $Y^{TTX} = \frac{I}{\Sigma}$  and  $Y^{TXX} = W = \Omega - \Omega_F$ .

We also have

$$\delta^2 J^\mu = \frac{1}{\sqrt{-g}} \partial_\nu(\sqrt{-g}\delta^2 F^{\mu\nu}) = 0. \quad (\text{B21})$$

We find three components of the Lorentz force vanish as

$$\delta^2 f_T^L = \delta J^\mu \delta F_{T\mu} = \frac{1}{\sqrt{-g}} \partial_\nu(\sqrt{-g}Y^{\mu\lambda\nu})\Omega_F \partial_\mu\psi, \quad (\text{B22})$$

$$\delta^2 f_X^L = \delta J^\mu \delta F_{X\mu} = 0, \quad (\text{B23})$$

$$\delta^2 f_\Psi^L = \delta J^\mu \delta F_{\Psi\mu} = 0, \quad (\text{B24})$$

because of  $\delta J^\rho = 0$ . The  $\rho$ -component of the Lorentz force is calculated as,

$$\begin{aligned} \delta^2 f_\rho^L &= \delta J^\mu \delta F_{\rho\mu} = \frac{1}{\sqrt{-g}} \partial_\nu(\sqrt{-g}Y^{\mu\lambda\nu}\partial_\lambda\psi)\partial_\mu\psi \\ &= \frac{1}{\sqrt{-g}} \sum_{\lambda=T,X} [-\partial_X(\sqrt{-g}Y^{T\lambda X}\partial_\lambda\psi)\partial_T\psi + \partial_T(\sqrt{-g}Y^{T\lambda X}\partial_\lambda\psi)\partial_X\psi] \\ &= \frac{1}{\sqrt{-g}} [-\partial_X(\Theta\partial_T\psi) + \partial_T(\Theta\partial_X\psi)], \end{aligned} \quad (\text{B25})$$

where  $\Theta = \sqrt{-g}Y^{T\alpha X}\partial_\alpha\psi = -\frac{IX}{\alpha^2}\partial_T\psi - R^2(\Omega_F - \Omega)\partial_X\psi$ . Here, we have the relation,

$$\delta^2 f_L^T = \Omega_F \delta^2 f_L^\rho. \quad (\text{B26})$$

To vanish  $\delta^2 f_\rho^L$  over the entire radial range ( $X > r_H$ ),  $\Theta$  should be zero. When  $\Theta$  is zero,  $I$ ,  $\Omega_F$ , and  $\Omega$  are zero. Then, only when  $I$ ,  $\Omega_F$ , and  $a_*$  are all zero,  $\delta^2 f_\rho^L$  vanishes. Then, except for the case of  $I$ ,  $\Omega_F$ ,  $a_*$ , the Alfvén wave induces the fast wave.

C. THE ENERGY DENSITY AND ENERGY FLUX DENSITY CORRECTED BY  $\chi$ 

We show the details of the calculation of the energy density and energy flux of Alfvén wave and the induced fast wave described by  $\chi$ . The Alfvén wave and the fast wave are given by the following perturbation, respectively,

$$\phi_1 = \bar{\phi}_1 + \delta\phi_1 = \Psi + \psi(T, X), \quad (\text{C27})$$

$$\phi_2 = \bar{\phi}_2 + \delta^2\phi_2 = \rho - \Omega_{\text{F}}T + \chi(T, X). \quad (\text{C28})$$

To derive time evolution equation of  $\chi$ , we use Eq. (2). When we take  $i = 2$ , we find the trivial equation:

$$\partial_\lambda(\sqrt{-g}W^{\lambda\alpha\mu\beta}\partial_\alpha\bar{\phi}_1\partial_\beta\chi)\partial_\mu\bar{\phi}_2 + \partial_\lambda(\sqrt{-g}W^{\lambda\alpha\mu\beta}\partial_\alpha\bar{\phi}_1\partial_\beta\bar{\phi}_2)\partial_\mu\chi = -\partial_\lambda(\sqrt{-g}W^{\lambda z\rho\beta}\partial_\beta\chi) - \partial_\lambda(\sqrt{-g}W^{\lambda z\mu\rho}\partial_\mu\chi) = 0. \quad (\text{C29})$$

When we take  $i = 1$ , we obtain the equation of  $\chi$ :

$$\begin{aligned} & \partial_\lambda(\sqrt{-g}W^{\lambda\alpha\mu\beta}\partial_\alpha\psi\partial_\beta\bar{\phi}_2)\partial_\mu\psi + \partial_\lambda(\sqrt{-g}W^{\lambda\alpha\mu\beta}\partial_\alpha\bar{\phi}_1\partial_\beta\chi)\partial_\mu\bar{\phi}_1 \\ &= \partial_\lambda(\sqrt{-g}Y^{\lambda\alpha\mu}\partial_\alpha\psi)\partial_\mu\psi + \partial_\lambda(\sqrt{-g}W^{\lambda\Psi\beta}\partial_\beta\chi) \\ &= \partial_\lambda(-\sqrt{-g}g^{\lambda\beta}\partial_\beta\psi) + \partial_\lambda(\sqrt{-g}W^{\lambda\alpha\mu\rho}\partial_\alpha\psi)\partial_\mu\psi = 0. \end{aligned} \quad (\text{C30})$$

Then, we obtain the time evolution equation of  $\chi$ ,

$$\square(g^{\Psi\Psi}\chi) = \nabla_\mu\nabla^\mu(g^{\Psi\Psi}\chi) = \frac{1}{\sqrt{-g}}\partial_\lambda(\sqrt{-g}g^{\Psi\Psi}g^{\mu\beta}\partial_\beta\chi) = \frac{1}{\sqrt{-g}}\partial_\lambda(\sqrt{-g}Y^{\lambda\alpha\mu}\partial_\alpha\psi\partial_\mu\psi) \equiv s, \quad (\text{C31})$$

where  $\square \equiv \nabla_\mu\nabla^\mu$  is the d'Alembertian. When we consider  $\chi$ , we found the force-free condition recovers as follows. When we take  $\nu \neq \rho$ , we have

$$\delta^2 f_\nu = \delta J^\mu \delta F_{\nu\mu} + \delta^2 J^\mu \bar{F}_{\nu\mu} = \delta J^\rho \delta F_{\nu\rho} + \delta^2 J^\rho \bar{F}_{\nu\rho} = 0. \quad (\text{C32})$$

Otherwise, we have

$$\begin{aligned} \delta^2 f_\rho &= \delta J^\mu \delta F_{\rho\mu} + \delta^2 J^\mu \bar{F}_{\rho\mu} = -\frac{1}{\sqrt{-g}}\partial_\nu(\sqrt{-g}Y^{\mu\lambda\nu}\partial_\lambda\psi)\partial_\mu\psi + \delta^2 J^z \\ &= -\frac{1}{\sqrt{-g}}\partial_\nu(\sqrt{-g}g^{\Psi\Psi}g^{\nu\beta}\partial_\beta\chi) + \frac{1}{\sqrt{-g}}\partial_\nu(\sqrt{-g}Y^{\nu\lambda\mu}\partial_\lambda\psi\partial_\mu\psi) = 0. \end{aligned} \quad (\text{C33})$$

Eventually, introducing  $\chi$ , we recovered and confirmed the force-free condition up to the second order perturbation.

We show the detail derivation of the equilibrium, first order, and second order of the values with respect to the conservation law. With respect to the energy density, we have

$$\begin{aligned}\bar{S}^T &= -\frac{1}{2}\bar{F}^{Ti}\bar{F}_{Ti} + \frac{1}{4}\bar{F}^{ij}\bar{F}_{ij} = \frac{1}{2}(Y^{\Psi\Psi\rho} + \Omega_{\text{F}}Y^{\Psi\Psi T}) = \frac{1}{2\Delta\Sigma} \left[ \alpha^2 - R^2(\Omega^2 - \Omega_{\text{F}}^2) + \frac{1}{\Sigma}I^2X^2\sin^2\theta \right] \\ \delta S^T &= -\frac{1}{2}\delta F^{Ti}\bar{F}_{Ti} - \frac{1}{2}\bar{F}^{Ti}\delta F_{Ti} + \frac{1}{4}\delta F^{ij}\bar{F}_{ij} + \frac{1}{4}\bar{F}^{ij}\delta F_{ij} = \left( Y^{\Psi\Psi\rho} + \frac{1}{2}\Omega_{\text{F}}Y^{\Psi\Psi T} \right) \partial_{\Psi}\psi = 0, \quad (\text{C35}) \\ \delta^2 S^T &= -\frac{1}{2}\delta F^{Ti}\delta F_{Ti} + \frac{1}{4}\delta F^{ij}\delta F_{ij} - \frac{1}{2}\bar{F}^{iT}\delta^2 F_{Ti} + \frac{1}{4}\bar{F}^{ij}\delta^2 F_{ij} + \frac{1}{4}\delta^2 F^{ij}\bar{F}_{ij} \\ &= -\frac{1}{2}[Y^{T\lambda\rho}\partial_T\psi + (Y^{\rho\lambda i} + \Omega_{\text{F}}Y^{T\lambda i})\partial_i\psi]\partial_{\lambda}\psi + Y^{\Psi\Psi j}\partial_j\chi + \Omega_{\text{F}}W^{\Psi\Psi\kappa T}\partial_{\kappa}\chi \\ &= \frac{1}{\Sigma} \left[ \frac{1}{2}\lambda(\partial_T\psi)^2 + \frac{1}{2}\{\alpha^2 + R^2(\Omega_{\text{F}}^2 - \Omega^2)\}(\partial_X\psi)^2 \right] + \frac{1}{\alpha^2}\Omega_{\text{F}}I\partial_X\psi\partial_T\psi + \frac{1}{\Sigma}(I\partial_X\chi - \frac{1}{\alpha^2}\Omega_{\text{F}}\partial_X\chi) \quad (\text{C36})\end{aligned}$$

With respect to the energy flux, we have

$$\bar{S}^X = \bar{F}^{Xi}\bar{F}_{iT} = \Omega_{\text{F}}Y^{\Psi\Psi X} = \frac{X^2}{\Sigma^2}I\Omega_{\text{F}}\sin^2\theta, \quad (\text{C37})$$

$$\delta S^X = \delta F^{Xi}\bar{F}_{iT} + \bar{F}^{Xi}\delta F_{iT} = \Omega_{\text{F}}^2Y^{\Psi\Psi X}\partial_{\Psi}\psi = 0, \quad (\text{C38})$$

$$\begin{aligned}\delta^2 S^X &= \delta F^{Xi}\delta F_{iT} + \bar{F}^{Xi}\delta^2 F_{iT} = \delta F^{X\rho}\delta F_{\rho T} + \bar{F}^{X\Psi}\delta^2 F_{\Psi T} \\ &= -Y^{X\lambda\rho}\partial_{\lambda}\psi\partial_T\psi - Y^{\Psi\Psi X}\partial_T\chi + \Omega_{\text{F}}W^{\Psi\Psi X\kappa}\partial_{\kappa}\chi \\ &= -\frac{1}{\Sigma}\partial_T\psi \left[ \frac{2MaIX}{\Delta}\partial_T\psi + \{\alpha^2 + R^2\Omega(\Omega_{\text{F}} - \Omega)\partial_X\psi \right] + \frac{1}{\Sigma} \left[ -I\partial_T\chi + \frac{\Delta}{X^2}\Omega_{\text{F}}\partial_X\chi \right]. \quad (\text{C39})\end{aligned}$$

With respect to the angular momentum, we introduced  $\chi$  to recover the force-free condition of the Alfvén wave up to second order of the perturbation so that we become able to consider the conservation law of angular momentum up to second order. The axial Killing vector  $\xi_{(\rho)}^{\mu} = (0, 0, 1, 0)$  yields the 4-angular momentum flux density  $M^{\mu} = \xi_{(\rho)}^{\nu}T_{\nu}^{\mu}$ , and we obtain the angular momentum conservation law in the corotating natural coordinates,

$$\nabla_{\mu}M^{\mu} = \frac{1}{\sqrt{-g}}\partial_{\mu}(\sqrt{-g}M^{\mu}) = \frac{\partial M^0}{\partial T} + \frac{1}{\sqrt{-g}}\frac{\partial}{\partial X}(\sqrt{-g}M^X) = \xi_{(\rho)}^{\mu}f_{\mu}^{\text{L}} = f_{\rho}^{\text{L}} = 0. \quad (\text{C40})$$

The 4-angular momentum density  $M^{\mu}$  in the corotating natural coordinates calculated as

$$M^{\mu} = \xi_{(\rho)}^{\nu}T_{\nu}^{\mu} = T_{\rho}^{\mu} = F^{\mu\nu}F_{\rho\nu}. \quad (\text{C41})$$



Then, we have the 4-angular momentum density of the equilibrium, first and second-order perturbations of the linear Alfvén wave,

$$\bar{M}^\mu = \bar{T}^\mu_\rho = \bar{F}^{\mu\lambda} \bar{F}_{\rho\lambda} = Y^{\Psi\Psi\mu}, \quad (\text{C42})$$

$$\delta M^\mu = \delta F^{\mu\nu} \bar{F}_{\rho\nu} + \bar{F}^{\mu\nu} \delta F_{\rho\nu} = \delta F^{\mu\Psi} \bar{F}_{\rho\Psi} + \bar{F}^{\mu\Psi} \delta F_{\rho\Psi} = -\delta F^{\mu\Psi} - Y^{\Psi\Psi\mu} \partial_\Psi \psi = 0, \quad (\text{C43})$$

$$\begin{aligned} \delta^2 M^\mu &= \delta^2 F^{\mu\nu} \bar{F}_{\rho\nu} + \delta F^{\mu\nu} \delta F_{\rho\nu} + \bar{F}_{\mu\nu} \delta^2 F^{\rho\nu} = \delta^2 F^{\mu\Psi} \bar{F}_{\rho\Psi} + \bar{F}^{\mu\Psi} \delta^2 F_{\rho\Psi} + \delta F^{\mu\nu} \delta F_{\rho\nu} \\ &= -\delta^2 F^{\mu\Psi} - Y^{\Psi\Psi\mu} \delta^2 F_{\rho\Psi} + \delta F^{\mu\nu} \delta F_{\rho\nu} \\ &= Y^{\mu\lambda\nu} \partial_\lambda \psi (-\Omega_F \delta_\nu^T \partial_\rho \psi - \partial_\nu \psi) + W^{\Psi\Psi\mu\kappa} \partial_\kappa \chi + Y^{\Psi\Psi\mu} \partial_\rho \chi = -Y^{\mu\lambda\nu} \partial_\lambda \psi \partial_\nu \psi + W^{\Psi\Psi\mu\kappa} \partial_\kappa \chi \end{aligned} \quad (\text{C44})$$

where we assume  $\mu \neq \Psi$ . Then, we confirm the conservation of the angular momentum for the second order of the perturbation as

$$\nabla_\mu \delta^2 M^\mu = \frac{1}{\sqrt{-g}} \partial_\lambda (\sqrt{-g} \delta^2 M^\lambda) = \frac{1}{\sqrt{-g}} \partial_\lambda [\sqrt{-g} (Y^{\nu\lambda\mu} \partial_\lambda \psi \partial_\nu \psi + W^{\Psi\Psi\mu\kappa} \partial_\kappa \chi)] = 0, \quad (\text{C45})$$

where we used Eq. (C44). We have the energy density and energy flux density of the equilibrium, first and second-order perturbations of the linear Alfvén wave distinctively,

$$\bar{M}^T = Y^{\Psi\Psi T}, \quad \bar{M}^X = Y^{\Psi\Psi X}, \quad (\text{C46})$$

$$\delta M^T = 0, \quad \delta M^X = 0, \quad (\text{C47})$$

$$\delta^2 M^T = -Y^{T\lambda\nu} \partial_\lambda \psi \partial_\nu \psi + W^{\Psi\Psi T\kappa} \partial_\kappa \chi = -Y^{T\lambda X} \partial_\lambda \psi \partial_X \psi + g^{\Psi\Psi} g^{T\kappa} \partial_\kappa \chi, \quad (\text{C48})$$

$$\delta^2 M^X = -Y^{X\lambda\nu} \partial_\lambda \psi \partial_\nu \psi + W^{\Psi\Psi X\kappa} \partial_\kappa \chi = Y^{T\lambda X} \partial_\lambda \psi \partial_T \psi + g^{\Psi\Psi} g^{X\kappa} \partial_\kappa \chi. \quad (\text{C49})$$

#### D. THE ENERGY TRANSPORT WITH WAVES

We recovered the force-free condition with the additional variable  $\chi$  so that we have the energy and momentum conservation,  $\nabla_\nu T^{\mu\nu} = 0$  up to the second order of the perturbations. When we use the time-like Killing vector  $\xi_{(T)}^\mu = (1, 0, 0, 0)$ , we have the energy conservation law,

$$\nabla_\nu S^\nu = \frac{1}{\sqrt{-g}} \partial_\nu (\sqrt{-g} S^\nu) = \frac{1}{\sqrt{-g}} \partial_T (\sqrt{-g} S^T) + \frac{1}{\sqrt{-g}} \partial_i (\sqrt{-g} S^i) = 0, \quad (\text{D50})$$

where  $S^\nu = -\xi_{(T)}^\mu T^{\mu\nu}$  is the 4-energy flux density. In the case of axisymmetry and translation symmetry with respect to the  $\Psi$ -direction, we have

$$\frac{\partial}{\partial T} (\sqrt{-g} S^T) + \frac{\partial}{\partial X} (\sqrt{-g} S^X) + \frac{\partial}{\partial \Psi} (\sqrt{-g} \delta^2 S^\Psi) = 0. \quad (\text{D51})$$

Here, we have  $\delta^2 S^\Psi = \delta^{1+1} S^\Psi = -\delta F^{\Psi j} \delta F_{Tj} = -Y^{\Psi \lambda j} \partial_\lambda \psi (\delta_j^\rho \partial_T \psi + \Omega_F \partial_j \psi) = -Y^{\Psi \Psi j} \partial_\Psi \psi (\delta_j^\rho \partial_T \psi + \Omega_F \partial_j \psi) = -(Y^{\Psi \Psi \rho} \partial_T \psi + \Omega_F Y^{\Psi \Psi X} \partial_X \psi) \partial_\Psi \psi$ , and Eq. (D51) and  $\partial_\Psi^2 \psi = -\psi$  yield the conservation expression,

$$\frac{\partial}{\partial T}(\sqrt{-g} \delta^2 e^\infty) + \frac{\partial}{\partial X}(\sqrt{-g} \delta^2 S_P) = 0, \quad (\text{D52})$$

where  $\delta^2 e^\infty = \delta^2 S^T + \frac{1}{2} Y^{\Psi \Psi \rho} \psi^2$  and  $\delta^2 S_P = \delta^2 S^X + \frac{1}{2\sqrt{-g}} \Omega_F I \psi^2$ . It reads,

$$\begin{aligned} & \int_{T_1}^{T_2} dT \int_{X_1}^{X_2} \frac{\partial}{\partial T}(\sqrt{-g} \delta^2 e^\infty) + \int_{T_1}^{T_2} dT \int_{X_1}^{X_2} \frac{\partial}{\partial X}(\sqrt{-g} \delta^2 S_P) \\ &= \int_{X_1}^{X_2} \sqrt{-g} \delta^2 e^\infty(X, T_2) - \int_{X_1}^{X_2} \sqrt{-g} \delta^2 e^\infty(X, T_1) + \int_{T_1}^{T_2} dT \sqrt{-g} \delta^2 S_P(X_2, T) - \int_{T_1}^{T_2} dT \sqrt{-g} \delta^2 S_P(X_1, T) = 0. \end{aligned} \quad (\text{D53})$$

When we define the total energy between  $X = X_1$  and  $X = X_2$  and the energy flux at  $X = X_b$  ( $b = 1, 2$ ) by

$$\delta^2 E(T) = \int_{X_1}^{X_2} \sqrt{-g} \delta^2 e^\infty(X, T) dX, \quad (\text{D54})$$

$$\delta^2 F_b(T) = \int_{T_1}^T \sqrt{-g} \delta^2 S_P(X_b, T') dT', \quad (\text{D55})$$

respectively, we obtain the conservation quantity as

$$\delta^2 E(T) - \delta^2 F_1(T) + \delta^2 F_2(T) = \delta^2 E(0). \quad (\text{D56})$$

Note that the energy of the Alfvén wave is conserved in the corotating magnetic natural frame  $(T', X', \Psi', \rho')$ ,

$$\delta^{1+1} E'(T) - \delta^{1+1} F'_1(T) + \delta^{1+1} F'_2(T) = \delta^{1+1} E'(0), \quad (\text{D57})$$

where  $\delta^{1+1} E'(T) = \int_{X_1}^{X_2} \sqrt{-g} \delta^{1+1} e^{\infty'}(X, T) dX$  and  $\delta^{1+1} F'_b(T) = \int_0^T \sqrt{-g} \delta^{1+1} S'_P(X_b, T') dT'$  ( $b = 1, 2$ ).

## E. THE NUMERICAL METHOD USED FOR THE 1-D WAVE EQUATION

Equations (18) with the additional term  $-\kappa(x)\psi$  in its right-hand side and Eq. (26) are written by multi-dimensional time-development equations as,

$$\begin{aligned}
 \frac{\partial\psi}{\partial T} &= -\frac{1}{\lambda(x)}\frac{\partial}{\partial x}(\xi + 2V\psi) - \frac{K}{\lambda}\zeta + \frac{1}{\lambda}\frac{\partial V}{\partial X}\psi, \\
 \frac{\partial\xi}{\partial T} &= -S\frac{\partial\psi}{\partial X}, \\
 \frac{\partial\zeta}{\partial T} &= \psi, \\
 \frac{\partial\chi}{\partial T} &= -\alpha^2\frac{\partial v}{\partial X} + \sigma, \\
 \frac{\partial v}{\partial T} &= -\frac{\Delta}{\Sigma}\frac{\partial\chi}{\partial X}, \\
 \frac{\partial\sigma}{\partial T} &= g(X),
 \end{aligned} \tag{E58}$$

where  $\xi(X, T)$ ,  $\zeta(X, T)$ ,  $v(X, T)$ , and  $\sigma(X, T)$  are new variables and  $g(x) = \frac{-\alpha^2\sqrt{-g}}{g^{TT}}s$ .

We use the two-step Lax-Wendroff scheme for the multi-dimension time-development equation

$$\frac{\partial\mathbf{u}}{\partial t} = -\mathbf{h} \odot \frac{\partial\mathbf{w}}{\partial X} + \mathbf{f}, \tag{E59}$$

where  $\mathbf{u}$  is the array of the conserved quantity density,  $\mathbf{w}$  is the array of the flux density of the conserved quantity,  $\mathbf{f}$  is the array of the source density of the conserved variable:

$$\mathbf{u}_j^{\overline{n+1}} = \mathbf{u}_j^n - \frac{\Delta t}{\Delta x}\mathbf{h}_j^n \odot (\mathbf{w}_{j+1}^n - \mathbf{w}_j^n) + \Delta t\mathbf{f}_j^n, \tag{E60}$$

$$\mathbf{u}_j^{n+1} = \frac{1}{2} \left[ \mathbf{u}_j^n \mathbf{u}_j^{\overline{n+1}} - \frac{\Delta t}{\Delta x}\mathbf{h}_j^n \odot (\mathbf{w}_j^{\overline{n+1}} - \mathbf{w}_{j-1}^{\overline{n+1}}) + \Delta t\mathbf{f}_j^{\overline{n+1}} \right]. \tag{E61}$$

Here, we used  $\odot$  to express the product of two vectors  $\mathbf{a} = (a_1, a_2, \dots)^T$  and  $\mathbf{b} = (b_1, b_2, \dots)^T$ ,

$$\mathbf{a} \odot \mathbf{b} \equiv \begin{pmatrix} a_1 b_1 \\ a_2 b_2 \\ \vdots \end{pmatrix}. \tag{E62}$$

Equation (E58) are given by

$$\mathbf{u} = \begin{pmatrix} \psi \\ \xi \\ \zeta \\ \chi \\ v \\ \sigma \end{pmatrix}, \mathbf{h} = \begin{pmatrix} \frac{1}{\lambda(x)} \\ S \\ 1 \\ \alpha^2 \\ \frac{\Delta}{\Sigma} \\ 1 \end{pmatrix}, \mathbf{w} = \begin{pmatrix} \xi + 2V\psi \\ \psi \\ 0 \\ v \\ \chi \\ 0 \end{pmatrix}, \mathbf{f} = \begin{pmatrix} -\frac{1}{\lambda} \left( \zeta - \frac{\partial V}{\partial X} \psi \right) \\ 0 \\ \psi \\ \sigma \\ 0 \\ g \end{pmatrix}. \quad (\text{E63})$$

To perform the precise calculation near the horizon, we use the tortoise coordinates,  $x$  defined by  $\frac{dX}{dx} = 1 - \frac{r_{\text{H}}}{X}$ . In the calculations in this paper, we use the tortoise coordinate,  $x = X - 2M + r_{\text{H}} \log(X - r_{\text{H}})/(2M - r_{\text{H}})$ , where the  $x = 0$  corresponds to the static limit ( $X = 2M$ ). The multidimensional equation (E59) is replaced by  $\frac{\partial \mathbf{u}}{\partial T} = -\frac{dx}{dX} \mathbf{h} \odot \frac{\partial}{\partial X} \mathbf{w} + \mathbf{f}$ , and then  $\mathbf{h}$  of Eq. (E59) is replaced by  $\frac{dx}{dX} \mathbf{h}$ .